

A Gaussian effective theory for gluon saturation

Edmond Iancu^a, Kazunori Itakura^{a,b}, and Larry McLerran^c

^a *Service de Physique Theorique, CE Saclay, F-91191 Gif-sur-Yvette*

^b *RIKEN BNL Research Center, BNL, Upton NY 11973*

^c *Nuclear Theory Group, Brookhaven National Laboratory, Upton, NY 11973*

Abstract

We construct a Gaussian approximation to the effective theory for the Colour Glass Condensate which describes correctly the gluon distribution both in the low density regime at high transverse momenta (above the saturation scale Q_s), and in the high density regime below Q_s , and provides a simple interpolation between these two regimes. At high momenta, the effective theory reproduces the BFKL dynamics, while at low momenta, it exhibits gluon saturation and, related to it, colour neutrality over the short distance scale $1/Q_s \ll 1/\Lambda_{QCD}$. Gauge-invariant quantities computed within this approximation are automatically infrared finite.

1 Introduction

There has been significant progress towards the understanding of the high energy, or small- x , limit of QCD in the recent years, and part of this progress is associated with the construction of an effective theory for the small- x gluons in the hadron light-cone wavefunction: the effective theory for the *Colour Glass Condensate* (CGC) [1, 2, 3, 4, 5, 6, 7, 8, 9] (see also Refs. [10, 11] for recent reviews and more references). This is an *effective* theory since it applies to gluons with a given value of the longitudinal momentum fraction x , with $x \ll 1$, and is obtained after integrating out the gluons with larger values of x within QCD perturbation theory.

The general strategy behind this construction is reminiscent of the Born–Oppenheimer approximation (i.e., there is a separation of scales between “fast” and “slow” degrees of freedom), and the resulting mathematical description is that of a *glass*. The “fast” degrees of freedom are the gluons (or, generally, partons) with larger values of x , which do not participate directly in the high-energy scattering (because of their large relative rapidities), but act as sources for the small- x gluons which produce the scattering. The “slow” degrees of freedom are the small- x gluons themselves, which have low rapidities (of the same order as the external projectile), but large densities in the impact parameter space (the transverse plane), since their radiative production is enhanced at small- x .

This whole partonic system is characterized by weak coupling — since the high gluon density acts as a hard scale for the running of the QCD coupling α_s —, but strong interactions with the small- x gluons, because these latter have densities which are parametrically of order $1/\alpha_s$. The crucial simplification, which allows for the all-order resummation of the density-enhanced interactions, is that the small- x gluons can be treated in the classical approximation [1], because of their large occupation numbers. That is, the small- x gluons can be described as the classical colour fields radiated by fast moving “colour sources” which represent the partons with larger values of x . Then, the all-order resummations alluded to before amount to treating the non-linear effects associated with these classical fields *exactly*, both in the classical field equations [1, 2, 3, 4], and in the quantum calculations involved in the construction of the effective theory [6, 7].

A second simplification, coming from the separation of scales between “fast” and “slow”, is that the internal dynamics of the fast partons can be neglected over the characteristic time scales for the dynamics at small x . This is the premise of the “glassy” description : For the purposes of the small- x physics, the fast partons can be treated as a *frozen* configuration of classical colour sources, which is *random*, in the sense that it can be any of the configurations allowed by the dynamics of the fast partons, and which must be *averaged over* in the calculation of physical quantities. This averaging is necessary also to restore gauge symmetry: on the average, the colour charge density must vanish at any point. This means that the *weight function* for this averaging, i.e., the probability density for having a given configuration of the colour sources, must be a gauge-invariant functional of the colour charge density. Further characterizing this functional, and deriving an explicit expression for it, will be our general objective in this paper.

This weight function encodes all the information about the colour source and its correlations, as inherited from the quantum dynamics at larger values of x . When x is further decreased, the structure of the classical field equations does not change: these are always the Yang–Mills equations with a colour source in their right hand side. What do change, are the correlations of the colour source, that is, its functional weight function. This change can be computed in perturbation theory, and expressed as a functional *renormalization group equation* (RGE) for the weight function [6, 7]. The initial condition for this equation is non-perturbative, and requires a model. But once this is specified, then the effective theory at scale x is completely determined by the solution to the RGE.

Even though the general solution to this equation is not known (this is a complicated non-linear equation [7]; see, however, [12]), its physical implications are well understood, at least, in some limiting kinematical regimes, where approximate solutions have been obtained [8, 10]. One has thus identified two important physical regimes: (I) a low-density regime at high transverse momenta (for fixed x), where the non-linear effects can be expanded out, and the RGE reduces to the BFKL evolution [13], and (II) a high-density regime at low transverse momenta, where the non-linearities are essential, and the RGE predicts *gluon saturation* [14, 15, 16]. The transition between these two regimes occurs at transverse momenta of the order of the “saturation scale” $Q_s(x)$, which is the typical momentum of the saturated gluons, and grows like a power of $1/x$ [17, 18, 19, 20].

These conclusions are corroborated by analytic [21, 22, 18, 9] and numerical [22, 23, 24, 25] studies of the Balitsky–Kovchegov (BK) equation [26, 21], which describes deep inelastic scattering at high energy, and is encoded too in the RGE [7]. Originally, the BK equation has been derived in a different approach [27, 28, 26, 21, 17, 29, 30, 31] (see also Refs. [14, 15] for earlier versions of this equation), which focuses on the observables through which an external projectile couples to a hadronic target, rather than on the wavefunction of the target itself.

Our purpose in this paper is to use the conclusions of these previous studies to construct an approximate solution to the RGE which is simply a *Gaussian* in the colour charge density ρ . Clearly, having an explicit expression for the weight function, which is moreover a Gaussian, will greatly facilitate the use of the CGC effective theory in practical calculations. In fact, with such a weight function, most calculations within the effective theory can be done quasi-analytically¹. Besides, a Gaussian weight function can be easily implemented in numerical simulations, like those performed in Ref. [32], where the effective theory is used to study nucleus–nucleus collisions on a lattice.

The adequacy of a Gaussian approximation may look at first surprising, given the highly non-linear structure of the RGE. By definition, a Gaussian approximation retains only the 2-point correlation function $\langle \rho\rho \rangle$ among all the n -point functions of the colour sources. Thus, this is a reasonable approximation provided (a) one disposes of a good approximation for the 2-point function, and (b) the higher n -point correlations are rela-

¹Note that, even with a Gaussian weight function, the CGC effective theory remains non-trivial, since the classical field equations (i.e., the Yang–Mills equations with colour source ρ) are non-linear. Still, as we shall remind in Sect. 2, the exact solution to these equations is known in analytic form.

tively weak. But in the RGE, the evolution of the 2–point function is generally mixed with that of the higher n –point functions, so it is not a priori clear how to construct a sensible approximation for the 2–point function alone (and thus a Gaussian weight function). It is even less clear whether such an approximation can be relevant for the non–linear regime, where higher correlations may be important as well.

Still, as we shall demonstrate below, a Gaussian weight function can accommodate both the BFKL evolution of the gluon distribution at high transverse momenta, and the phenomenon of gluon saturation at low transverse momenta. It is only the transition between these two regimes that cannot be accurately described in this way. (But our approximation will provide a smooth interpolation between these limiting regimes.) To understand when, and to which extent, is a Gaussian approximation expected to work, let us make a few remarks that will get substantiated in the subsequent analysis:

In the low–density regime at high transverse momenta $k_{\perp} \gg Q_s(x)$, the evolution generated by the RGE does not couple correlation functions with different number of external legs. In particular, the 2–point function $\langle \rho\rho \rangle$ satisfies a closed equation, which is moreover linear [6]. This is the BFKL equation [13]. By solving this equation, one can construct a Gaussian weight function which incorporates correctly the BFKL dynamics for both the unintegrated gluon distribution, and deep inelastic scattering.

In the saturation regime at low momenta $k_{\perp} \ll Q_s(x)$, the colour sources and the radiated fields are typically strong (their amplitudes are parametrically of order $1/g$), so the dynamics is fully non–linear. Remarkably, however, the non–linear effects drop out completely from the RGE. This is related to the specific way how these effects enter the RGE in the first place [7] : they enter only via *Wilson lines*, that is, path–ordered exponentials of the classical fields. At saturation, where the fields are strong, these complex exponentials oscillate rapidly and average to zero, together with all their correlations, when probed over transverse distances of the order of the saturation length $1/Q_s(x)$, or larger. Thus, in this high–density regime, the RGE becomes effectively *quadratic*², and can be trivially solved. The resulting weight function is then truly a Gaussian [8].

We see an interesting duality emerging at saturation: this strong field regime allows for a description in terms of a Gaussian weight function, so like a free theory.

Another important feature at saturation is *colour neutrality* [8, 9, 10, 33] : The saturated gluons shield each other in such a way that their global colour charge vanishes when integrated over a disk of radius $1/Q_s(x)$, or larger. This is expressed by the following property of the charge–charge correlator: $\langle \rho(k_{\perp})\rho(-k_{\perp}) \rangle \propto k_{\perp}^2$ for momenta $k_{\perp} \ll Q_s(x)$. This property has crucial implications:

First of all, it is synonymous of saturation: As we shall see, $\langle \rho(k_{\perp})\rho(-k_{\perp}) \rangle/k_{\perp}^2$ is essentially the unintegrated gluon distribution. Thus, the fact that the charge–charge correlator is proportional to k_{\perp}^2 at low momenta, means that the unintegrated gluon distribution is independent of k_{\perp} (up to logarithms), which is saturation indeed. In fact,

²In the same sense, for instance, as the Hamiltonian for a quantum–mechanical harmonic oscillator is a quadratic operator.

we shall see that the scale $Q_s(x)$ is primarily generated (by the non-linear effects in the quantum evolution) as the typical scale for colour neutrality. Then this becomes also the “saturation scale” because of the connection between the distribution of the colour sources and that of the small- x gluons alluded to above.

Second, colour neutrality ensures that gauge-invariant quantities come out infrared finite when computed in the effective theory. This should be contrasted with the original McLerran–Venugopalan (MV) model [1], in which the colour sources are assumed to be uncorrelated, so the corresponding charge–charge correlator $\langle \rho(k_\perp) \rho(-k_\perp) \rangle$ is independent of k_\perp . Because of that, the calculation of physical quantities like the gluon distribution function [3], or the dipole–hadron scattering amplitude [10], within this model meets with logarithmic infrared divergences. It has been proposed by Lam and Mahlon [5] to remove these divergences by imposing colour neutrality on the size of the nucleon, that is, by effectively taking into account the non-perturbative mechanism of confinement. In Ref. [32], this suggestion has been implemented in numerical simulations, but the results turn out to be quite sensitive to the poorly known non-perturbative physics. As we shall show in this paper, when the colour neutrality due to saturation is taken into account, all such infrared divergences are eliminated already at the perturbative scale $1/Q_s(x)$.

Other effects which can be attributed to colour neutrality at saturation, and which illustrate the lack of infrared sensitivity of the effective theory, are the suppression of the “infrared diffusion” in the quantum evolution towards small x (this has been verified in the numerical simulations of the BK equation [24]), and the predominance of the short-range scattering in the evolution of the total cross-sections with increasing energy [9].

Note that colour neutrality is a weaker property than confinement: Although the global colour charge vanishes indeed, the multipolar moments (starting with the dipolar one) are still non-zero, and generate long range interactions. But the latter die away sufficiently fast to ensure the infrared finiteness of all observables for high-energy scattering (at fixed impact parameter). The information about confinement is needed only in the calculation of the total cross-section, since this requires an integration over *all* impact parameters [9, 34, 35]. Still, as shown in Ref. [9] on the example of the dipole–hadron scattering, by combining the non-linear evolution equations with a minimal assumption about confinement in the initial conditions, one can compute the rate for the increase of the total cross-section with the energy, and conclude that σ_{tot} saturates the Froissart bound [36] at very high energy. Similar conclusions have been reached in Refs. [34, 37].

In view of the previous considerations, our general strategy in this paper should be clear by now: We shall construct our Gaussian approximation for the weight function by requiring its kernel $\langle \rho \rho \rangle$ to satisfy the BFKL equation at high momenta, to describe colour neutrality at low momenta, and to interpolate smoothly between these two limiting regimes, with the change in behaviour occurring at the saturation scale. The last condition requires a saturation criterion for the charge–charge correlator, that we shall formulate, and prove to be equivalent to the other criteria used in the literature. For practical purposes, we shall propose also a simplified form of the kernel, in which the general solution to the BFKL equation is replaced by its “geometric scaling” approximation [18],

valid up to momenta $k_{\perp} \sim Q_s^2(x)/\Lambda_{QCD}$.

To test the quality of our approximation, we shall compute the unintegrated gluon distribution and the dipole–hadron scattering amplitude, and find the expected results at both high and low momenta. In particular, from the kernel of the Gaussian, we shall deduce a simple analytic formula for the unintegrated gluon distribution, which has a *scaling* form, i.e., it is a function of $k_{\perp}/Q_s(x)$, and interpolates smoothly between saturation at $k_{\perp} < Q_s(x)$ and BFKL behaviour at $k_{\perp} > Q_s(x)$.

Also, we shall derive a phenomenologically useful formula for the dipole–hadron scattering amplitude, which properly incorporates the constraints of geometric scaling [38] (both in the saturation regime, and in the scaling window [18] above $Q_s(x)$), and the colour neutrality due to saturation. This analytic formula can be easily applied to the description of electron–hadron deep inelastic scattering, as an alternative to the more phenomenological parametrizations proposed in Refs. [39, 40].

At this point, let us note an important difference in the mechanism of saturation between the Gaussian effective theory that we shall construct and the original MV model [1], which has a Gaussian weight function too: In the MV model, the colour sources are uncorrelated, and the saturation arises exclusively via the non–linear effects in the Yang–Mills dynamics of the classical fields. By contrast, in the effective theory which includes quantum evolution, the saturation is the consequence of the long–range spatial correlations between the colour sources, and, as such, it is encoded already in the weight function. This explains why, in our case, the unintegrated gluon distribution can be simply proportional to the kernel of the Gaussian even in the non–linear regime at saturation.

This paper is organized as follows: In Section 2, we shall succinctly review the effective theory for the CGC, and introduce the notations and conventions to be used throughout. In Section 3, we show that Gaussian approximations for the weight function can be formally generated through *mean field approximations* to the RGE. In Section 4, we briefly describe the MV model [1, 2, 3, 5], which will serve as a basis of comparison for the following developments. In Section 5, we discuss the simplifications which occur in the RGE in the limiting situations where the transverse momenta are either very large, or very small, compared to the saturation scale. This justifies the use of a Gaussian approximation in these regimes, at least. In Section 6, we construct an approximation for the charge–charge correlator which interpolates smoothly between the limiting behaviours found previously. This specifies the Gaussian effective theory completely. In Section 7, we use this effective theory to first derive a simple expression for the unintegrated gluon distribution, and then compute the dipole–hadron scattering amplitude. Our conclusions are summarized in Section 8.

2 The Colour Glass Condensate

2.1 The classical effective theory

Let us summarize here the equations at the basis of the effective theory for the CGC. The classical field obeys the Yang–Mills equations with a colour current due to the fast partons³ :

$$(D_\nu F^{\nu\mu})_a(x) = \delta^{\mu+} \rho_a(x^-, x_\perp). \quad (2.1)$$

The structure of the colour current in the r.h.s. is fixed by the kinematics: *i*) The current has just a plus component ($J_a^\mu \simeq \delta^{\mu+} \rho_a$) since the fast partons move nearly at the speed of light in the positive z (or positive x^+) direction. *ii*) By Lorentz contraction, the support of the colour charge density ρ_a is concentrated near the light–cone, i.e., near $x^- = 0$. *iii*) By Lorentz time dilation, ρ_a is independent of the light–cone time x^+ , i.e., it is “frozen”, according to the terminology used in the Introduction.

All the approximations involved in writing eq. (2.1) are consistent with the quantum evolution towards small- x in the leading–log approximation, since this evolution preserves the separation of scales in longitudinal momenta (and therefore also in time).

The observables that can be computed in the effective theory are the gauge–invariant correlations of the gauge fields. These are first evaluated on the solution $A^\mu[\rho]$ to eq. (2.1), and the result is then averaged over all the configurations of ρ , with a gauge–invariant weight function $W_\tau[\rho]$ which depends upon x via the rapidity variable $\tau \equiv \ln(1/x)$.

For instance, we shall need later the scattering amplitude for the high energy scattering between a “colour dipole” (say, a quark–antiquark pair in a colourless state) and the hadron. This quantity is a physical observable (at least, indirectly) in the sense that it enters the formula for the F_2 structure function at small x [27, 41]. In the eikonal approximation, the scattering amplitude is obtained as [42, 26] :

$$\begin{aligned} \mathcal{N}_\tau(x_\perp, y_\perp) &= 1 - S_\tau(x_\perp, y_\perp), \quad S_\tau(x_\perp, y_\perp) \equiv \frac{1}{N_c} \left\langle \text{tr} \left(V^\dagger(x_\perp) V(y_\perp) \right) \right\rangle_\tau, \\ \left\langle \text{tr} \left(V^\dagger(x_\perp) V(y_\perp) \right) \right\rangle_\tau &= \int D\rho W_\tau[\rho] \text{tr} \left(V_{x_\perp}^\dagger[\rho] V_{y_\perp}[\rho] \right), \end{aligned} \quad (2.2)$$

where $V^\dagger(x_\perp)$ and $V(y_\perp)$ are Wilson lines describing the interactions between the fast moving quark, or antiquark, from the dipole and the colour field in the hadron:

$$V^\dagger(x_\perp) \equiv \text{P exp} \left\{ ig \int dx^- A_a^+(x^-, x_\perp) t^a \right\}, \quad (2.3)$$

³We recall that, in light–cone coordinates, and with our present conventions, $x^+ \equiv (t+z)/\sqrt{2}$ plays the role of the light–cone time, while $x^- \equiv (t-z)/\sqrt{2}$ is the longitudinal coordinate. Correspondingly, k^- is the light–cone energy, and k^+ is the longitudinal momentum; thus, $x = k^+/P^+$, where k^+ refers to a parton in the hadron, while P^+ denotes the total longitudinal momentum of the hadron.

and $A_a^+ \equiv A_a^+[\rho]$ is the projection of the classical colour field along the trajectory of the quark (or the antiquark). The Wilson line correlator in eq. (2.2) is written in a suitable gauge in which the component A^+ is non-zero, but the result is actually gauge-independent, since this correlator can be completed to a Wilson loop by joining the points x_\perp and y_\perp via Wilson lines in the transverse planes at $x^- = \pm\infty$ (where the transverse fields A^i can be chosen to vanish in any gauge with $A^+ \neq 0$).

Explicit calculations are most conveniently performed in the covariant gauge $\partial_\mu A_a^\mu = 0$, since in this gauge the solution A^μ to the classical equation (2.1) has only one non-trivial component: $A_a^+ = \delta^{\mu+} \alpha_a$, with α_a satisfying the two-dimensional Poisson equation:

$$-\nabla_\perp^2 \alpha_a(x^-, x_\perp) = \rho_a(x^-, x_\perp). \quad (2.4)$$

This simplification reflects the fact that the classical field radiated by ρ has only one non-trivial field strength, namely the “electric field” F_a^{+i} , which in the covariant gauge is computed as $-\partial^i \alpha_a$. The corresponding result in other gauges is then obtained via the appropriate gauge rotation. Particularly interesting for what follows is the result in the light-cone (LC) gauge $A_a^+ = 0$, which reads (in matrix notations; see [7, 10] for details) :

$$F^{+i}(x^-, x_\perp) = U(-\partial^i \alpha) U^\dagger, \quad (2.5)$$

where

$$U^\dagger(x^-, x_\perp) = \text{P exp} \left\{ ig \int_{-\infty}^{x^-} dz^- \alpha(z^-, x_\perp) \right\}, \quad (2.6)$$

is the matrix for the gauge rotation from the covariant gauge to the LC gauge. This is essentially the same Wilson line as for the quark scattering in the eikonal approximation, eq. (2.3). Note that eqs. (2.4)–(2.6) provide an explicit expression for the electric field in the LC gauge in terms of the colour source ρ_a in the covariant gauge. In this sense, the solution to the classical field equations (2.1) is known *exactly* (in any gauge).

Eq. (2.4) can be easily inverted :

$$\begin{aligned} \alpha_a(x^-, x_\perp) &= \int d^2 y_\perp \langle x_\perp | \frac{1}{-\nabla_\perp^2} | y_\perp \rangle \rho_a(x^-, y_\perp) \\ &= \int \frac{d^2 y_\perp}{4\pi} \ln \frac{1}{(x_\perp - y_\perp)^2 \Lambda^2} \rho_a(x^-, y_\perp). \end{aligned} \quad (2.7)$$

The infrared cutoff Λ is necessary to invert the Laplacian in two dimensions, but, as we shall see, it disappears in the calculation of physical quantities. From eq. (2.7), it is clear that the “Coulomb field” $\alpha(x^-, x_\perp)$ is time-independent and localized near $x^- = 0$, like the colour source.

To summarize, to compute the dipole-hadron scattering amplitude (2.2) within the effective theory, one has to replace $A_a^+ \rightarrow \alpha_a$ in eq. (2.3), with α_a given by eq. (2.7), and then perform the functional integral over ρ in the second line of eq. (2.2), with the weight function $W_\tau[\rho]$ (which for this purpose is needed as a functional of the colour source ρ_a in the covariant gauge).

2.2 The Renormalization Group Equation at Small x

When decreasing x (or increasing the rapidity $\tau \equiv \ln(1/x)$), new quantum modes become relatively “fast”, and must be included in the effective source at the new value of x . This operation modifies both the longitudinal support of ρ (with increasing τ , the colour source extends to larger and larger values of the x^-), and its correlations. All these changes can be absorbed into a functional renormalization of the weight function $W_\tau[\rho]$, which therefore depends upon τ . To the order of interest, this dependence is governed by a functional *renormalization group equation*, which reads [6, 7] :

$$\frac{\partial W_\tau[\rho]}{\partial \tau} = \frac{1}{2} \int_{x_\perp, y_\perp} \frac{\delta}{\delta \rho_\tau^a(x_\perp)} \chi_{ab}(x_\perp, y_\perp)[\rho] \frac{\delta}{\delta \rho_\tau^b(y_\perp)} W_\tau[\rho], \quad (2.8)$$

with $\chi[\rho]$ a positive definite functional of ρ , whose explicit form is not needed here (this can be found in Refs. [7, 8, 10]), but whose relevant properties will be discussed below.

Eq. (2.8) allows one to construct the weight function by integrating out the quantum gluons in layers of τ . The kernel $\chi[\rho]$ encodes the changes in the correlations of the colour source induced at one step in this construction, and depends upon the source ρ created in all the previous steps. Indeed, the quantum gluons which are integrated out in one step propagate through the background field $A[\rho]$ of the colour source generated in the previous steps. In general, this classical field is strong, so its non-linear effects on the dynamics of the quantum gluons must be included exactly. Because of that, the functional $\chi[\rho]$ is non-linear in ρ to all orders, and also non-local, both in the longitudinal coordinates, and in the transverse ones. In fact, the non-linearity in ρ and the non-locality in x^- are strongly correlated, since they have a common origin: namely, the fact that $\chi[\rho]$ depends upon ρ via the Wilson lines in eq. (2.3).

There is one more notation in eq. (2.8) which waits for an explanation: this is the argument $\rho_\tau^a(x_\perp)$ of the functional derivatives there. This is a notation for the colour charge density $\rho^a(x^-, x_\perp)$ at a specific longitudinal location $x^- = x_\tau^-$, which is the upper boundary of the support of the classical source in x^- . That is, the colour source at rapidity τ has support within a limited interval in x^- , namely at $0 < x^- < x_\tau^-$, with $x_\tau^- \propto e^\tau$.

This correlation between the quantum evolution in τ and the longitudinal extent of the colour charge distribution can be understood as a consequence of the uncertainty principle: Since obtained by integrating out quantum modes with large longitudinal momenta $p^+ \gg xP^+ \equiv e^{-\tau}P^+$, the classical source at rapidity τ must be localized near $x^- = 0$, within a distance $\Delta x^- \sim e^\tau x_0^-$ (with $x_0^- \equiv 1/P^+$).

But eq. (2.8) shows that this correlation is even stronger: Namely, it shows that, when the rapidity is further increased, say from τ to $\tau + d\tau$, the additional contribution to the colour source which is generated in this way has *no overlap* in x^- with the original source at rapidity τ . Rather, this new contribution makes a new layer in x^- , which is located between x_τ^- and $x_{\tau+d\tau}^-$. This is why the functional derivatives in eq. (2.8) involve just the colour source $\rho_\tau \equiv \rho(x_\tau^-)$ in this outermost layer.

To conclude, when integrating out the quantum modes in layers of τ , one builds the colour source in layers of x^- , with a one-to-one correspondence between the x^- coordinate

of a given layer in ρ and the rapidity τ of the modes that have been integrated out to generate that layer.

This correspondence is most simply formulated if one uses the *space-time rapidity* y ,

$$y \equiv \ln(x^-/x_0^-), \quad x_0^- \equiv 1/P^+, \quad -\infty < y < \infty, \quad (2.9)$$

to indicate the longitudinal coordinate of a field. We shall set, e.g.,

$$\begin{aligned} \rho_y^a(x_\perp) &\equiv x^- \rho^a(x^-, x_\perp) \quad \text{for } x^- = x_y^- \equiv x_0^- e^y, \\ \int dy \rho_y^a(x_\perp) &= \int dx^- \rho^a(x^-, x_\perp), \end{aligned} \quad (2.10)$$

and similarly for α , eq. (2.7), or any other field. Eq. (2.3) is then rewritten as :

$$V^\dagger(x_\perp) = \text{P exp} \left\{ ig \int dy \alpha_y^a(x_\perp) t^a \right\}. \quad (2.11)$$

Then, the previous discussion shows that the space-time rapidity y of a given layer in ρ is identical to the usual (momentum) rapidity of the fast gluons that have produced that layer. In particular, the colour source created by the quantum evolution up to τ has support at space-time rapidities $y \leq \tau$ (in agreement with the simple argument based on the uncertainty principle). This is important since, as we shall see, the τ -dependence of the observables computed in the effective theory comes precisely from the upper limit on the longitudinal support of ρ . The Colour Glass evolves by expanding in y .

3 The Gaussian approximation

The exact solution to eq. (2.8) is certainly not a Gaussian. The kernel $\chi[\rho]$ in this equation is non-linear in ρ to all orders, so the complete solution $W_\tau[\rho]$ must be non-linear as well, for any initial condition. (This non-linearity is manifest on the formal representation of the solution derived in Ref. [12].) Still, as mentioned in the Introduction, there are interesting situations in which a weight function which is a Gaussian in ρ may capture the relevant physics. Before describing such physical situations in more detail, in Sections 4 and 5, let us first characterize the general structure of a Gaussian weight function, and show how to obtain such a Gaussian approximation for $W_\tau[\rho]$, at least at a formal level, via mean field approximations to the non-linear RGE (2.8) (see also Ref. [8]).

We start by displaying the most general Gaussian weight function which is consistent with gauge symmetry, and respects the correspondence between space-time rapidity and momentum rapidity explained in the previous section. In the covariant gauge, in which both the classical solution and the kernel $\chi[\rho]$ are known explicitly, this Gaussian reads:

$$W_\tau[\rho_y^a(x_\perp)] = \mathcal{N}_\tau \exp \left\{ -\frac{1}{2} \int_{-\infty}^{\tau} dy \int_{x_\perp, y_\perp} \frac{\rho_y^a(x_\perp) \rho_y^a(y_\perp)}{\lambda_y(x_\perp, y_\perp)} \right\} \times \delta_\tau[\rho], \quad (3.1)$$

where $\delta_\tau[\rho]$ is a δ -functional enforcing that $\rho_y \equiv 0$ for any $y > \tau$, and \mathcal{N}_τ is a numerical factor, which ensures the right normalization:

$$\int D\rho W_\tau[\rho] = 1, \quad (3.2)$$

but is irrelevant for the computation of correlation functions.

Note that the information about the longitudinal support of ρ_y is included in the weight function. Thus, when computing observables by averaging over ρ with this weight function, like in eq. (2.2), the support of ρ_y will be restricted to $y \leq \tau$, as it should.

For physical space-time rapidities $y \leq \tau$, eq. (3.1) is indeed a Gaussian in ρ , with the following 2-point function :

$$\langle \rho_y^a(x_\perp) \rho_{y'}^b(y_\perp) \rangle_\tau = \delta^{ab} \delta(y - y') \theta(\tau - y) \lambda_y(x_\perp, y_\perp), \quad (3.3)$$

which is local in space-time rapidity, but generally non-local in the transverse coordinates. This is the most general non-local structure which is allowed by gauge symmetry, as we explain now: For $W_\tau[\rho]$ to be gauge-invariant, the colour sources $\rho_y^a(x_\perp)$ at different points (y, x_\perp) must be connected by appropriate gauge links, or “Wilson lines”. In the covariant gauge, in which eq. (3.1) is explicitly written, the gauge potential has just a plus component, $A_a^+ \equiv \alpha_a$, so the only non-trivial gauge links are those in the longitudinal direction, cf. eq. (2.3). And, indeed, the kernel $\chi[\rho]$ of the RGE is built with such Wilson lines [7, 10], and thus is consistent with gauge symmetry, but also non-linear in ρ to all orders. For the gauge-invariance to be preserved in the Gaussian approximation, where no Wilson lines are permitted, $W_\tau[\rho]$ must be *local* in y , as shown in eq. (3.1).

The Gaussian weight function (3.1) obeys the following evolution equation:

$$\frac{\partial W_\tau[\rho]}{\partial \tau} = \frac{1}{2} \int_{x_\perp, y_\perp} \lambda_\tau(x_\perp, y_\perp) \frac{\delta^2 W_\tau[\rho]}{\delta \rho_\tau^a(x_\perp) \delta \rho_\tau^a(y_\perp)}. \quad (3.4)$$

By comparison with eq. (2.8), one sees that, at a formal level, the Gaussian approximation is tantamount to replacing the general kernel $\chi[\rho]$ in the RGE by the ρ -independent, but τ -dependent, quantity λ_τ .

To determine the kernel λ_τ of the Gaussian, which is also the 2-point function in the present approximation, we shall require this quantity to obey the “mean field version” of the actual evolution equation satisfied by the complete 2-point function $\langle \rho(1)\rho(2) \rangle_\tau$. Here, by “mean field version”, we mean that the correlations which enter this equation are evaluated with the Gaussian weight function (3.1) itself. This gives a self-consistent approximation for the 2-point function.

Since the general 2-point function $\langle \rho_y^a(x_\perp) \rho_{y'}^b(y_\perp) \rangle_\tau$ is not local in y , nor diagonal in colour, it is preferable to consider the equation satisfied by the following quantity:

$$\mu_\tau(x_\perp, y_\perp) \equiv \frac{1}{N_c^2 - 1} \langle \rho^a(x_\perp) \rho^a(y_\perp) \rangle_\tau, \quad (3.5)$$

where

$$\rho^a(x_\perp) \equiv \int dy \rho_y^a(x_\perp) \quad (3.6)$$

is the effective colour charge density in the transverse plane, as obtained after integrating over the longitudinal profile of the hadron.

In the Gaussian approximation, eq. (3.3) immediately implies:

$$\mu_\tau(x_\perp, y_\perp) = \int_{-\infty}^{\tau} dy \lambda_y(x_\perp, y_\perp), \quad \text{or} \quad \lambda_\tau(x_\perp, y_\perp) = \frac{\partial \mu_\tau}{\partial \tau}(x_\perp, y_\perp). \quad (3.7)$$

In general, the evolution equation for the two-point function (3.5) can be obtained from its definition:

$$\langle \rho^a(x_\perp) \rho^b(y_\perp) \rangle_\tau \equiv \int D\rho W_\tau[\rho] \rho^a(x_\perp) \rho^b(y_\perp), \quad (3.8)$$

by first taking a derivative with respect to τ , then using eq. (2.8) for $\partial W_\tau / \partial \tau$, and finally performing a couple of functional integrations by parts. This yields:

$$\frac{\partial}{\partial \tau} \langle \rho^a(x_\perp) \rho^b(y_\perp) \rangle_\tau = \langle \chi^{ab}(x_\perp, y_\perp) \rangle_\tau + \langle \sigma^a(x_\perp) \rho^b(y_\perp) \rangle_\tau + \langle \rho^a(x_\perp) \sigma^b(y_\perp) \rangle_\tau, \quad (3.9)$$

where the quantity $\sigma^a(x_\perp)$ has been generated as the functional derivative of $\chi[\rho]$:

$$\sigma^a(x_\perp)[\rho] \equiv \frac{1}{2} \int d^2 y_\perp \frac{\delta \chi^{ab}(x_\perp, y_\perp)}{\delta \rho_\tau^b(y_\perp)}. \quad (3.10)$$

It is useful to recall here that, in the quantum calculation leading to eq. (3.3) [6, 7], $\sigma[\rho]$ represents the “virtual correction” (i.e., the sum of the self-energy and vertex corrections), and is complementary to the “real correction” represented by $\chi[\rho]$. The relation (3.10) between these two quantities [30, 7] is very important, since it ensures that the evolution equations for gauge-invariant observables derived from eq. (2.8) are infrared finite.

In general, both χ and σ are non-linear in ρ , so eq. (3.9) is not a closed equation — it couples the 2-point function to higher n -point functions of ρ —, but only the first in an infinite hierarchy of coupled evolution equations. A closed equation can be nevertheless obtained in the *mean field approximation* (MFA) in which the correlation functions in eq. (3.9) are evaluated with the Gaussian weight function (3.1). Then, eq. (3.9) reduces to the following equation for $\lambda_\tau = \partial \mu_\tau / \partial \tau$ (cf. eq. (3.7)) :

$$\lambda_\tau(x_\perp, y_\perp) = \langle \chi(x_\perp, y_\perp) + \sigma(x_\perp) \rho(y_\perp) + \rho(x_\perp) \sigma(y_\perp) \rangle_\tau, \quad (3.11)$$

where $\langle \chi \rangle \equiv \langle \chi^{aa} \rangle / (N_c^2 - 1)$, etc., and the expectation value in the r.h.s. is computed with the weight function (3.1), so it is a known functional of λ_y . In general, this functional is very non-linear and also non-local, but it considerably simplifies in the limiting cases of interest (see Sect. 5 below).

To summarize, our MFA is defined by the weight function (3.1) with the kernel λ_τ determined self-consistently by eq. (3.11). This is more general than the MFA considered in Ref. [8], which was an approximation on the evolution Hamiltonian (the functional differential operator in the r.h.s. of eq. (2.8)) :

$$H \equiv -\frac{1}{2} \frac{\delta}{\delta \rho_\tau} \chi[\rho] \frac{\delta}{\delta \rho_\tau} \longrightarrow \bar{H} \equiv -\frac{1}{2} \langle \chi[\rho] \rangle_\tau \frac{\delta^2}{\delta \rho_\tau \delta \rho_\tau}. \quad (3.12)$$

In eq. (3.12), the kernel $\chi[\rho]$ in the Hamiltonian is simply replaced by its average over ρ , so its functional derivative $\sigma[\rho]$ is implicitly neglected, and eq. (3.11) reduces to

$$\lambda_\tau(x_\perp, y_\perp) = \langle \chi(x_\perp, y_\perp) \rangle_\tau, \quad (3.13)$$

as is also obvious by comparing eqs. (3.4) and (3.12). The reason why eq. (3.11) appears to be more complete, is that, in its derivation, the equation for the 2–point function has been first generated with the *full* Hamiltonian, and the MFA has been implemented only afterwards. By contrast, eq. (3.13) has been generated directly with an approximate form of the Hamiltonian.

As we shall discuss in Sect. 5, the difference between eqs. (3.11) and (3.13) has important consequences. In particular, eq. (3.13) is not good enough for our present purposes. Rather, our final approximation for the weight function, to be constructed in Sect. 6, will be based on eq. (3.11).

We conclude this section by displaying the expression for the dipole-hadron scattering amplitude (2.2) in the Gaussian approximation. The Wilson lines in eq. (2.11) involve the Coulomb field $\alpha_y^a(x_\perp)$, which is linearly related to the colour charge density (cf. eq. (2.4)), and therefore is itself a Gaussian random variable, with 2–point function (cf. eq. (3.3)) :

$$\langle \alpha_y^a(x_\perp) \alpha_{y'}^b(y_\perp) \rangle_\tau = \delta^{ab} \delta(y - y') \theta(\tau - y) \gamma_y(x_\perp, y_\perp), \quad (3.14)$$

where

$$\gamma_y(x_\perp, y_\perp) \equiv \int d^2 z_\perp d^2 u_\perp \langle x_\perp | \frac{1}{-\nabla_\perp^2} | z_\perp \rangle \lambda_y(z_\perp, u_\perp) \langle u_\perp | \frac{1}{-\nabla_\perp^2} | y_\perp \rangle. \quad (3.15)$$

From eqs. (2.11) and (3.14), a straightforward calculation yields [3, 10] :

$$S_\tau(x_\perp, y_\perp) = \exp \left\{ -\frac{g^2 C_R}{2} \int_{-\infty}^{\tau} dy \left[\gamma_y(x_\perp, x_\perp) + \gamma_y(y_\perp, y_\perp) - 2\gamma_y(x_\perp, y_\perp) \right] \right\}. \quad (3.16)$$

The colour factor C_R is $C_F = (N_c^2 - 1)/2N_c$ for a dipole made of a quark and an antiquark (this is the relevant case for γ^*p deep inelastic scattering), and $C_A = N_c$ for a gluonic dipole, which is interesting for the discussion of the RGE (since the Wilson lines which enter the kernel $\chi[\rho]$ are written in the adjoint representation, i.e., they refer to gluons).

Eq. (3.16) simplifies if one assumes the hadron to be homogeneous in the transverse plane, within a disk of radius R , with R much larger than any transverse separation $x_\perp - y_\perp$ of interest (so that one can neglect the edge effects). Then, the various 2–point functions

depend only upon the relative coordinate: e.g., $\lambda_y(x_\perp, y_\perp) = \lambda_y(r_\perp)$, with $r_\perp \equiv x_\perp - y_\perp$, and it is convenient to introduce the Fourier transform:

$$\lambda_y(k_\perp) = \int d^2r_\perp e^{-ik_\perp \cdot r_\perp} \lambda_y(r_\perp), \quad (3.17)$$

and similarly for the other functions. The relation (3.15) simplifies to:

$$\gamma_\tau(k_\perp) = \frac{\lambda_y(k_\perp)}{k_\perp^4}, \quad (3.18)$$

while eq. (3.16) is finally rewritten as:

$$S_\tau(r_\perp) = \exp \left\{ -g^2 C_R \int_{-\infty}^{\tau} dy \int \frac{d^2k_\perp}{(2\pi)^2} \frac{\lambda_y(k_\perp)}{k_\perp^4} \left[1 - e^{ik_\perp \cdot r_\perp} \right] \right\}. \quad (3.19)$$

4 The McLerran-Venugopalan model

In this section, we interrupt our presentation of the quantum evolution and briefly review a simple Gaussian model for the weight function, originally proposed by McLerran and Venugopalan [1] to describe the gluon distribution of a large nucleus ($A \gg 1$) (see also [2, 3, 4, 5, 10]). There is no quantum evolution in this model (i.e., no dependence upon x), but this can be viewed as the initial condition, valid at some moderate value x_0 , for the quantum evolution towards smaller values of x .

In this model, the only colour sources are the $A \times N_c$ valence quarks, which are assumed to be uncorrelated, since they do not overlap with each other: Valence quarks which overlap in transverse projection belong typically to different nucleons, and thus have no overlap in the longitudinal direction, because of confinement. The distribution of these sources is therefore described by a Gaussian weight function, like in eq. (3.1), but with a kernel which is local also in the transverse coordinates:

$$W_{\tau_0}[\rho] = \mathcal{N}_\tau \exp \left\{ -\frac{1}{2} \int_{-\infty}^{\tau_0} dy \int_{x_\perp} \frac{\rho_y^a(x_\perp) \rho_y^a(x_\perp)}{\lambda_y(x_\perp)} \right\}. \quad (4.1)$$

Physically, the kernel $\lambda_y(x_\perp)$ represents the average colour charge squared of the valence quarks per unit space-time rapidity and per unit transverse area, at the given point (y, x_\perp) . It satisfies the sum rule:

$$\int dy \int d^2x_\perp \lambda_y(x_\perp) = \frac{g^2 C_F A N_c}{N_c^2 - 1} = \frac{g^2 A}{2}, \quad (4.2)$$

which follows since the total colour squared in the nucleus is $\langle Q^a Q^a \rangle = g^2 C_F A N_c$ (recall that the colour charge squared of a single quark is $g^2 t^a t^a = g^2 C_F$), with

$$Q^a \equiv \int dy \int d^2x_\perp \rho_y^a(x_\perp). \quad (4.3)$$

The y -dependence of the kernel $\lambda_y(x_\perp)$ remains unspecified in the MV model. This is not necessarily a problem since, when computed in this model, many interesting quantities (see, e.g., eq. (3.19)) involve only the colour charge integrated over y (cf. eqs. (3.5)–(3.7)):

$$\mu_0(x_\perp) \equiv \int_{-\infty}^{\tau_0} dy \lambda_y(x_\perp). \quad (4.4)$$

To get simple formulae, it is again convenient to assume transverse homogeneity within the nuclear disk of radius $R_A = R_0 A^{1/3}$ (this assumption can be relaxed, and actually is, in numerical simulations [32]). Then:

$$\mu_0(A) = \frac{g^2 A}{2\pi R_A^2} \propto A^{1/3}. \quad (4.5)$$

When the MV model is used to compute physical quantities, one usually finds logarithmic infrared divergences, which can be attributed to the fact that the Gaussian weight function (4.1) is local in x_\perp . Note that, when translated to momentum space, this locality means that the Fourier modes of λ_y are independent of k_\perp (cf. eq. (3.17)) :

$$\lambda_y(x_\perp, y_\perp) = \delta^{(2)}(x_\perp - y_\perp) \lambda_y \implies \lambda_y(k_\perp) = \lambda_y. \quad (4.6)$$

Consider then eq. (3.19) for the dipole scattering amplitude. In the MV model, it becomes:

$$S_0(r_\perp) = \exp \left\{ -g^2 C_R \int \frac{d^2 k_\perp}{(2\pi)^2} \frac{\mu_0}{k_\perp^4} \left[1 - e^{ik_\perp \cdot r_\perp} \right] \right\}, \quad (4.7)$$

and the integral over k_\perp in the exponent has a logarithmic infrared divergence indeed⁴.

Clearly, this divergence reflects the limitations of the assumptions underlying the MV model. In particular, the assumption that the colour sources are uncorrelated must fail for sufficiently large transverse separations. For instance, long-range correlations will certainly occur because of confinement: The three valence quarks within the same nucleon are bound in a colour singlet state, so the total colour charge (4.3), together with its higher multipolar moments, must vanish when measured over distances of the order of the nucleon size R_0 , or larger. This in turn requires the correlator $\lambda_y(k_\perp)$ to vanish at low momenta $k_\perp \lesssim 1/R_0$, in contradiction with eq. (4.6).

Based on this physical idea, it has been proposed [5] to cure the infrared problem of the MV model by imposing colour neutrality on the nucleon level. This means that, effectively, the integral over k_\perp in eq. (4.7) is cut off in the infrared at momenta of order $1/R_0 \sim \Lambda_{QCD}$. In fact, since the divergence is only logarithmic, then, to leading-log accuracy, the exact value of the cutoff is not important, neither are the details of the non-perturbative mechanism responsible for this screening. To evaluate eq. (4.7) to this

⁴The divergence is only logarithmic since, at small k_\perp , $1 - e^{ik_\perp \cdot r_\perp} \approx -ik_\perp \cdot r_\perp + (1/2)(k_\perp \cdot r_\perp)^2$, and the term linear in k_\perp vanishes after angular integration. This compensation of the leading IR divergence between 1 and $e^{ik_\perp \cdot r_\perp}$ is ultimately a consequence of the fact that the external probe is a colourless *dipole*, with a gauge-invariant S -matrix element.

accuracy, one can insert a sharp momentum cutoff equal to Λ_{QCD} , and also expand the exponential (since $k_\perp \cdot r_\perp \ll 1$ for this dominant contribution). One obtains [3, 10] :

$$S_0(r_\perp) \simeq \exp \left\{ -\frac{r_\perp^2 Q_0^2(A)}{4} \ln \frac{1}{r_\perp^2 \Lambda_{QCD}^2} \right\}, \quad (4.8)$$

with:

$$Q_0^2(A) \equiv \alpha_s C_R \mu_0(A) = \frac{2\alpha_s^2 C_R A^{1/3}}{R_0^2}. \quad (4.9)$$

Still, for the physical scales of interest (e.g., in relation with heavy ion collisions), the leading-log approximation above is not really satisfactory, and the complete, numerical results in Ref. [32] turn out to be quite sensitive to the specific assumptions about the non-perturbative physics (i.e., upon the prescription used to implement colour neutrality).

Thus, in this classical context, where the valence quarks are the only colour sources, one cannot avoid a rather strong sensitivity to the soft, non-perturbative physics. As we shall show in what follows, this sensitivity disappears once the effects of the quantum evolution are taken into account: At sufficiently large energies (or small enough values of x), the colour sources are predominantly *gluons*, and these gluons have long-range correlations associated with the non-linear (but still perturbative) physics of saturation, which ensure colour neutrality already over the short scale $1/Q_s \ll 1/\Lambda_{QCD}$.

5 Colour neutrality from quantum evolution

We now return to the quantum evolution described by eq. (2.8), and examine the validity of the Gaussian approximations obtained in Sect. 3 via formal manipulations. To this aim, we need to consider the structure of the kernel $\chi[\rho]$ in some detail. In fact, for the present purposes, it is enough to know that χ depends upon ρ via the Wilson lines (2.11), and that the strength of the field α in these Wilson lines is correlated with the gluon density in the system (see Sect. 7.1). This suggests different approximations at short and, respectively, large distances compared to the saturation length $1/Q_s$.

5.1 High k_\perp : The BFKL equation

For short distances $r_\perp \ll 1/Q_s(\tau)$, that is, for an external probe with a large transverse resolution $Q^2 = 1/r_\perp^2$ (e.g., a small dipole with transverse size r_\perp), scattering is dominated by gluons with relatively large transverse momenta ($k_\perp \gg Q_s(\tau)$), and thus a low density. In this *dilute* regime, the colour field is weak, $g\alpha \ll 1$, so one can expand the Wilson lines (2.11) in powers of $g\alpha$, and keep only the linear term in the expansion:

$$V^\dagger(x_\perp) \approx 1 + ig \int dy \alpha_y(x_\perp) \equiv 1 + ig\alpha(x_\perp). \quad (5.1)$$

After this expansion, $\chi[\rho]$ becomes quadratic in $\rho(x_\perp) \equiv \int dy \rho_y(x_\perp)$ (cf. eq. (3.6)) [6, 7]:

$$\chi[\rho] \approx \rho \mathcal{K} \rho, \quad (5.2)$$

which means that the corresponding RGE is still non-linear :

$$\frac{\partial W_\tau[\rho]}{\partial \tau} \approx \frac{1}{2} \frac{\delta}{\delta \rho} (\rho \mathcal{K} \rho) \frac{\delta}{\delta \rho} W_\tau[\rho]. \quad (5.3)$$

That is, even in the dilute regime at high k_\perp , the weight function $W_\tau[\rho]$ is, strictly speaking, *not* a Gaussian. Still, as compared to the general RGE (2.8), the evolution generated by eq. (5.3) exhibits an important simplification: it does not mix correlations $\langle \rho(1)\rho(2)\dots\rho(n) \rangle$ with different numbers n of colour sources [7].

In particular, eq. (5.3) provides a closed evolution equation for the 2–point function (3.5) — i.e., eq. (3.9) with $\chi[\rho] \approx \rho \mathcal{K} \rho$ and $\sigma[\rho] \approx \mathcal{K} \rho$ —, which is moreover *linear* [6]. When written in momentum space, this equation is recognized as the BFKL equation[13]:

$$\begin{aligned} \frac{\partial \mu_\tau(k_\perp)}{\partial \tau} &= \frac{\alpha_s N_c}{\pi^2} \int d^2 p_\perp \frac{k_\perp^2}{p_\perp^2 (k_\perp - p_\perp)^2} \mu_\tau(p_\perp) \\ &\quad - \frac{\alpha_s N_c}{2\pi^2} \int d^2 p_\perp \frac{k_\perp^2}{p_\perp^2 (k_\perp - p_\perp)^2} \mu_\tau(k_\perp). \end{aligned} \quad (5.4)$$

The emergence of the BFKL equation in this regime, and in the present approximations, is as expected, since the quantity $\mu_\tau(k_\perp)$ plays also the role of the unintegrated gluon distribution (see Sect. 7.1). The two terms in the r.h.s. are the “real” and, respectively, “virtual” BFKL corrections, and originate from the terms involving χ and, respectively, σ , in the r.h.s. of eq. (3.9). Since eq. (5.4) is local in rapidity, then, clearly, if $\mu_\tau(k_\perp)$ satisfies this equation, so does also $\lambda_\tau(k_\perp) = \partial \mu_\tau / \partial \tau$, which is the kernel of the Gaussian.

Let us now compare eq. (5.4) with the corresponding predictions of the mean field approximations introduced in Sect. 3, namely, eqs. (3.11) and (3.13).

In this low density regime, where χ is quadratic in ρ , while σ is linear, there is obviously no difference between the general equation (3.9) and its mean field approximation (3.11). Thus, the BFKL equation (5.4) is *exactly* reproduced by the linearized version of eq. (3.11). That is, although the general solution $W_\tau[\rho]$ to eq. (5.3) is *not* a Gaussian, our mean field approximation is still able to encode the evolution of the 2–point function correctly, because this evolution is linear, and it does not mix the 2–point function with higher n –point functions (i.e., because the BFKL Hamiltonian in the r.h.s. of eq. (5.3) is diagonal in the number of fields ρ).

It is also important to notice that, within this Gaussian effective theory, the BFKL evolution of the kernel λ_τ of the Gaussian gets transmitted to other 2–point functions of physical interest, like the dipole–hadron scattering amplitude (2.2). Specifically, in the linear approximation appropriate at high k_\perp , eq. (3.19) reduces to:

$$\mathcal{N}_\tau(r_\perp) = 1 - S_\tau(r_\perp) \approx g^2 N_c \int_{-\infty}^{\tau} dy \int \frac{d^2 k_\perp}{(2\pi)^2} \frac{\lambda_y(k_\perp)}{k_\perp^4} \left[1 - e^{i k_\perp \cdot r_\perp} \right]. \quad (5.5)$$

By taking a derivative with respect to τ in this equation, and using eq. (5.4) for $\lambda_\tau = \partial\mu_\tau/\partial\tau$, one can check, after some lengthy but straightforward manipulations, that the (linearized) scattering amplitude obeys to:

$$\frac{\partial}{\partial\tau} \mathcal{N}_\tau(r_\perp) = \bar{\alpha}_s \int \frac{d^2z_\perp}{\pi} \frac{r_\perp^2}{(r_\perp - z_\perp)^2 z_\perp^2} \left(\mathcal{N}_\tau(z_\perp) - \frac{1}{2} \mathcal{N}_\tau(r_\perp) \right), \quad (5.6)$$

which is the coordinate space form of the BFKL equation. This is further recognized as the linearized version of the Balitsky–Kovchegov (BK) equation, which is the general evolution equation for $\mathcal{N}_\tau(r_\perp)$ that follows from the RGE (2.8) [7], and also from other formalisms which focus on the evolution of the dipole wavefunction [26, 21, 29, 30, 31].

Consider also the MFA based on eq. (3.13) : Since this approximation misses the σ term, it fails to reproduce the “virtual” BFKL term, and thus the complete BFKL equation (5.4). This is a serious failure: as well known, the “virtual” term cancels the infrared divergence of the “real” term at $p_\perp = k_\perp$, and thus plays an important role in the BFKL dynamics.

Still, there exists a kinematical limit in which the “virtual” term becomes unimportant: this is high- k_\perp^2 regime where one retains only terms enhanced by both energy logs $\ln(1/x)$ and transverse momentum logs $\ln(k_\perp^2/\Lambda^2)$ (“double logarithmic approximation”, or DLA). This limit is common to the BFKL [13] and DGLAP [43] equations, and is formally obtained by assuming $p_\perp \ll k_\perp$ in eq. (5.4). In this limit, one expects the MFA based on eq. (3.13) to become appropriate. This is confirmed by the analysis in Ref. [8] which shows that, at very high k_\perp , the self-consistency equation (3.13) reduces to:

$$\lambda_\tau(k_\perp) = \frac{\alpha_s N_c}{\pi} \int_{-\infty}^{\tau} dy \int^{k_\perp^2} \frac{dp_\perp^2}{p_\perp^2} \lambda_y(p_\perp), \quad (5.7)$$

or, equivalently (cf. eq. (3.7)),

$$\frac{\partial\mu_\tau(k_\perp)}{\partial\tau} = \frac{\alpha_s N_c}{\pi} \int^{k_\perp^2} \frac{dp_\perp^2}{p_\perp^2} \mu_\tau(p_\perp), \quad (5.8)$$

which is recognized indeed as the DLA evolution equation (compare to eq. (5.4)).

It is important to keep in mind, however, that DLA is not the right approximation to study the approach towards saturation. Indeed, there is a large kinematical gap between the validity range for this approximation and the saturation line $k_\perp = Q_s(\tau)$ [18], and, within this gap, one can rely only on the full BFKL equation. This is why in what follows we shall focus exclusively (in this high momentum regime) on the BFKL dynamics.

5.2 Low k_\perp : Saturation and colour neutrality

At low transverse momenta $k_\perp \lesssim Q_s$, the gluons are *saturated*, that is, they have large occupation numbers $dN/d\tau d^2k_\perp \sim 1/\alpha_s$, and a radial momentum distribution $dN/d\tau dk_\perp$ which is peaked at the relatively hard scale $k_\perp \sim Q_s(\tau)$ (see Sect. 7.1). Thus, in the corresponding CGC description, the colour fields have large amplitudes⁵ $\alpha \sim 1/g$, and

⁵More precisely, we mean here the fields integrated over all rapidities, i.e., $\alpha(x_\perp) = \int dy \alpha_y(x_\perp)$.

carry typical momenta $k_\perp \sim Q_s$. Accordingly, the Wilson lines (2.11) — which are complex exponentials built with these fields — oscillate around zero over a characteristic distance $\sim 1/Q_s(\tau)$ in the transverse plane. This implies that Wilson lines which are separated by large distances $\gg 1/Q_s(\tau)$ are necessarily uncorrelated (since their relative phases are random). Thus, when studying the dynamics over large transverse separations $r_\perp \gg 1/Q_s(\tau)$, it should be a good approximation to neglect the correlations of the Wilson lines (or, more generally, to treat them as small quantities). This is the “random phase approximation” (RPA) introduced in Ref. [8, 30].

In this approximation, the RGE (2.8) simplifies drastically [8] : After neglecting the Wilson lines, the kernel χ becomes independent of ρ , and the corresponding solution $W_\tau[\rho]$ is truly a Gaussian (to the accuracy of the RPA). This is quite remarkable, given that, at saturation, we are in a strong field regime, where the dynamics is fully non-linear. Specifically, one finds [8]

$$\chi^{ab}(x_\perp, y_\perp) \approx \delta^{ab} \frac{1}{\pi} \langle x_\perp | -\nabla_\perp^2 | y_\perp \rangle \quad (\text{RPA}) \quad (5.9)$$

which gives the following RGE :

$$\frac{\partial W_\tau[\rho]}{\partial \tau} = \frac{1}{2} \int \frac{d^2 k_\perp}{(2\pi)^2} \frac{k_\perp^2}{\pi} \frac{\delta^2 W_\tau[\rho]}{\delta \rho_\tau^\alpha(k_\perp) \delta \rho_\tau^\alpha(-k_\perp)}, \quad (5.10)$$

where we recognize a Coulomb-like Hamiltonian in the r.h.s. A brief comparison with eq. (3.4) allows us to identify the charge-charge correlator at low k_\perp :

$$\lambda_y(k_\perp) = \frac{1}{\pi} k_\perp^2, \quad (k_\perp \ll Q_s(\tau)). \quad (5.11)$$

Clearly, both mean field approximations discussed in Sect. 3 reproduce eqs. (5.9)–(5.11) in the low- k_\perp limit.

Note that this low- k_\perp distribution is homogeneous in all the (longitudinal and transverse) coordinates. That is, in the transverse plane, it is only a function of the relative coordinate $x_\perp - y_\perp$, and in the longitudinal direction, it is independent of the space-time rapidity y . One should however keep in mind that, for given $k_\perp \ll Q_s(\tau)$, eq. (5.11) applies only for y in the interval $\tau_s(k_\perp) < y < \tau$, with $\tau_s(k_\perp)$ being the rapidity at which the saturation scale becomes equal to the momentum k_\perp of interest:

$$Q_s^2(\tau) = k_\perp^2 \quad \text{for} \quad \tau = \tau_s(k_\perp). \quad (5.12)$$

It follows that the integrated quantity (cf. eq. (3.7)) :

$$\mu_\tau(k_\perp) \Big|_{\text{sat}} = \int_{\tau_s(k_\perp)}^{\tau} dy \frac{k_\perp^2}{\pi} = \left(\tau - \tau_s(k_\perp) \right) \frac{k_\perp^2}{\pi}, \quad (k_\perp \ll Q_s(\tau)), \quad (5.13)$$

which measures the density of saturated colour sources (with given k_\perp) in the transverse plane, grows only *linearly* with τ , that is, logarithmically with the energy. This should

be contrasted with the rapid increase of the corresponding quantity at $k_\perp \gg Q_s(\tau)$, which evolves according to the BFKL equation (5.4), and thus rises exponentially with τ . Eq. (5.13) shows that, at low momenta $k_\perp \ll Q_s(\tau)$, the colour charge density *saturates*, because of the strong non-linear effects in the quantum evolution [8]. As we shall discuss in Sect. 7.1, this further implies the saturation of the gluon distribution. In Ref. [33], the result in eq. (5.13) has been reobtained from a study of the BK equation.

According to eq. (5.11), the only remaining correlations at saturation are those in the transverse separation r_\perp between the colour sources. Importantly, these are such as to ensure *colour neutrality* [10, 9, 33]. Indeed, the fact that $\lambda_y(k_\perp) \propto k_\perp^2$ when $k_\perp^2 \rightarrow 0$ implies $\langle \mathcal{Q}^a \mathcal{Q}^a \rangle = 0$, where \mathcal{Q}^a is the total colour charge (4.3) of the saturated gluons:

$$\langle \mathcal{Q}^a \mathcal{Q}^a \rangle_\tau = \int dy \lambda_y(k_\perp = 0) = 0. \quad (5.14)$$

Since the distribution of ρ at small k_\perp is a Gaussian, and both the 1-point function $\langle \mathcal{Q}^a \rangle$, and the 2-point function $\langle \mathcal{Q}^a \mathcal{Q}^a \rangle$, of \mathcal{Q}^a vanish when computed with this Gaussian, it follows that $\mathcal{Q}^a = 0$, which physically means that the saturated gluons are globally colour neutral. In fact, since the Wilson lines average to zero over a finite distance $\Delta x_\perp \gtrsim 1/Q_s(\tau)$, it follows that colour neutrality is achieved already over a transverse scale of the order of the saturation length (this can be explicitly verified by using eq. (5.11)):

$$\int dy \int_{\Delta S_\perp} d^2 x_\perp \rho_y^a(x_\perp) = 0, \quad (5.15)$$

where ΔS_\perp is, e.g., a disk of radius $R > 1/Q_s(\tau)$.

When $k_\perp \rightarrow 0$, the spectrum (5.11) vanishes sufficiently fast to ensure the infrared finiteness of the dipole scattering amplitude (3.19), and, more generally, of all the quantities which were, at most, linearly infrared divergent in the MV model. Thus, we expect that all the observables computed within the CGC effective theory come out infrared finite, and thus are insensitive to the non-perturbative physics at momenta $k_\perp \lesssim \Lambda_{QCD}$. In fact, because of saturation, the spectrum starts to soften already at momenta $k_\perp > Q_s$, where the linear, BFKL, evolution applies. This happens in the window for “geometric scaling” [18], to be discussed in Sect. 6.

5.3 Brief summary of the quantum evolution

To summarize, if we compare to the initial condition of the MV type — namely, the local Gaussian (4.1), which describes a system of independent colour sources —, the general effect of the quantum evolution is to introduce *correlations* in the transverse and longitudinal directions (i.e., non-localities in r_\perp and y), and *non-linearities* in ρ (i.e., higher n -point correlations among the colour sources). However, the role and the relative importance of the various non-local effects, and of the higher n -point functions, may differ from one kinematical regime to another.

At transverse momenta far above Q_s , the longitudinal correlations are irrelevant (they are always integrated out, as in eqs. (3.6) and (5.1)), and the various n -point correlations evolve independently from each other. In particular, the 2-point function evolves according to the BFKL equation (5.4), and so does the dipole-hadron scattering amplitude.

In the opposite limit at $k_\perp \lesssim Q_s$, the RGE becomes linear (cf. eq. (5.10)), and the weight function is strictly Gaussian, and therefore local in y . The only correlations which persist in this regime are the transverse correlations reflecting the colour neutrality of the saturated gluons. These are sufficient to ensure that gauge-invariant observables come out infrared finite when computed in the effective theory.

In the intermediate regime at $k_\perp \sim Q_s$, the evolution is fully non-linear — correlation functions of all orders get mixed in the evolution equations —, and therefore very non-local in y . Clearly, there is no hope to describe the complex physics in this transition regime via a Gaussian approximation. However, we expect this physics not to be essential for physical quantities for which the external resolution scale is either well above, or well below, the saturation scale. As we shall verify on the example of the dipole-hadron scattering amplitude in Sect. 7.2, such quantities receive most of their contributions from either the hard modes with $k_\perp \gg Q_s$, or the saturated gluons with $k_\perp \ll Q_s$.

To easily compute such observables, it would be advantageous to dispose of a Gaussian weight function which interpolates smoothly between the known behaviours at high and, respectively, low transverse momenta. For instance, the complete solution $\lambda_\tau(x_\perp, y_\perp)$ to the evolution equation in the MFA, eq. (3.11), would provide such an interpolation, since this is necessarily a smooth function and has the right limiting behaviours. But eq. (3.11) is a complicated, non-linear, integral equation, whose general solution can be obtained, at most, numerically. For practical calculations, it would be preferable to have a simple analytic interpolation, which satisfies the BFKL equation (5.4) at high k_\perp , and reduces to eq. (5.11) at low k_\perp , with the transition between the two regimes taking place at $k_\perp \sim Q_s$. Such an interpolation will be constructed in the next section.

6 The interpolation

So far, we have found the following limiting behaviours for the charge-charge correlator (3.3) at high and, respectively, low transverse momenta:

$$\bar{\lambda}_\tau(k_\perp) \approx \begin{cases} \lambda_\tau(k_\perp), & \text{for } k_\perp \gg Q_s(\tau) \\ \frac{1}{\pi} k_\perp^2, & \text{for } k_\perp \ll Q_s(\tau) \end{cases}. \quad (6.1)$$

Here, and from now on, we reserve the notation $\lambda_\tau(k_\perp)$ for the solution to the BFKL equation, and use $\bar{\lambda}_\tau(k_\perp)$ to denote the kernel of the Gaussian weight function (3.1).

Clearly, the following function provides a smooth interpolation between the limiting behaviours shown above:

$$\bar{\lambda}_\tau(k_\perp) \equiv \frac{k_\perp^2 \lambda_\tau(k_\perp)}{k_\perp^2 + \pi \lambda_\tau(k_\perp)}. \quad (6.2)$$

There is, however, one more constraint that eq. (6.2) must satisfy in order to be a physically acceptable interpolation: the change from the high-momentum regime to the low-momentum one must happen at the saturation scale. For the function in eq. (6.2), this condition is satisfied provided the two terms in the denominator become of similar magnitude when $k_\perp = Q_s(\tau)$:

$$\frac{1}{\pi} Q_s^2(\tau) \simeq \lambda_\tau(k_\perp = Q_s(\tau)). \quad (6.3)$$

Note that this is precisely the condition that the limiting behaviours shown in eq. (6.1) match quasi-continuously with each other at the saturation scale. Clearly, whether this condition is fulfilled or not, depends upon our definition of the saturation scale. Usually, $Q_s(\tau)$ is defined through a “saturation criterion”, imposed on the gluon “packing factor” in the transverse plane [14, 15, 16, 17], or, equivalently, on the dipole-hadron scattering amplitude [27, 22, 8, 18, 19, 9, 20]. For instance, in terms of $\mathcal{N}_\tau(r_\perp)$, the saturation criterion reads (κ is a number of order unity)

$$\mathcal{N}_\tau(r_\perp) = \kappa \quad \text{for} \quad r_\perp^2 = 1/Q_s^2(\tau), \quad (6.4)$$

which is the same as the condition that the dipole of transverse size equal to the saturation length is completely absorbed (“blackness”).

We shall argue below that, in fact, eq. (6.3) is just another definition of the saturation scale, equivalent to that in eq. (6.4). In other terms, the condition (6.3) is satisfied at the right saturation scale *by definition*, so eq. (6.2) is a physically acceptable interpolation indeed. Of course, such an interpolation is not unique, but at the present level of accuracy we cannot distinguish between different interpolations which are all physically acceptable according to the previous criteria. In what follows, we shall adopt the interpolation (6.2) because of its simplicity.

At a mathematical level, the equivalence between the two formulations of the saturation condition — in terms of the scattering amplitude, eq. (6.4), or in terms of the charge-charge correlator, eq. (6.3) — is almost obvious: Both $\mathcal{N}_\tau(r_\perp)$ and $\lambda_\tau(k_\perp)$ satisfy the BFKL equation and obey the same saturation criterion, namely, the relevant “scaling function” ($\mathcal{N}_\tau(r_\perp)$ in one case, and $\lambda_\tau(k_\perp)/k_\perp^2$ in the other) is constant on the saturation line $k_\perp = Q_s(\tau)$. Thus, it is a priori clear that eq. (6.3) will provide the correct estimate for $Q_s(\tau)$. Still, it is instructive to briefly develop the consequences of this equation here, in order not only to recover the known result for the saturation scale [17, 18], but also to establish a simple scaling approximation for $\lambda_\tau(k_\perp)$, which will greatly simplify the use of eq. (6.2) in practice.

For convenience, in what follows we shall mostly consider the solution to the BFKL equation (5.4) for the case of a *fixed* coupling α_s , and only briefly indicate the changes which occur when a running coupling $\alpha_s(Q_s^2)$ is used instead. Also, we shall need only the approximate form of the solution, which is obtained via a saddle point approximation in the Mellin transform of $\lambda_\tau(k_\perp)$ (see, e.g., [18] for details):

$$\lambda_\tau(k_\perp) \simeq f(\tau) \sqrt{Q_0^2 k_\perp^2} \exp \left\{ \omega \bar{\alpha}_s \tau - \frac{1}{2\beta \bar{\alpha}_s \tau} \left(\ln \frac{k_\perp^2}{Q_0^2} \right)^2 \right\}. \quad (6.5)$$

In this equation, $f(\tau)$ is a slowly varying function that will be ignored in what follows (since its contribution to $\ln(\lambda_\tau/k_\perp^2)$ is comparatively small), Q_0 is a scale of order Λ_{QCD} introduced by the initial conditions, $\bar{\alpha}_s \equiv \alpha_s N_c/\pi$, and ω and β are pure numbers: $\omega = 4 \ln 2 \approx 2.77$, $\beta = 28\zeta(3) \approx 33.67$.

Eq. (6.5) is strictly correct for $k_\perp \gg Q_s(\tau)$, where the colour charge density is low ($\lambda_\tau/k_\perp^2 \ll 1$), and BFKL is a right approximation. But this expression can be extrapolated down to $k_\perp \sim Q_s(\tau)$ (since BFKL remains marginally valid down to the saturation line), and then inserted in the saturation condition (6.3), to obtain an equation for $Q_s(\tau)$:

$$\sqrt{\frac{Q_0^2}{Q_s^2}} \exp \left\{ \omega \bar{\alpha}_s \tau - \frac{1}{2\beta \bar{\alpha}_s \tau} \left(\ln \frac{Q_s^2}{Q_0^2} \right)^2 \right\} \simeq 1. \quad (6.6)$$

This has the following solution :

$$Q_s^2(\tau) = Q_0^2 e^{c\bar{\alpha}_s\tau}, \quad c = [-\beta + \sqrt{\beta(\beta + 8\omega)}]/2 = 4.84\dots \quad (6.7)$$

which is the correct result [17, 18], as anticipated. Note that the factor in front of the exponential in eq. (6.7) is not under control in the present approximations. A more refined treatment [19, 20] shows that this prefactor has actually a weak dependence upon τ .

It is further interesting to study the behaviour of $\lambda_\tau(k_\perp)$ for momenta close to the saturation scale, where a simple approximation to eq. (6.5) can be obtained. To this aim, let us replace Q_0^2 by $Q_s^2(\tau)$ as the reference scale in eq. (6.5), by writing:

$$\ln \frac{k_\perp^2}{Q_0^2} = \ln \frac{k_\perp^2}{Q_s^2(\tau)} + c\bar{\alpha}_s\tau. \quad (6.8)$$

A simple calculation yields then:

$$\lambda_\tau(k_\perp) = \frac{1}{\pi} k_\perp^2 \exp \left\{ -\gamma \ln \frac{k_\perp^2}{Q_s^2(\tau)} - \frac{1}{2\beta \bar{\alpha}_s \tau} \left(\ln \frac{k_\perp^2}{Q_s^2(\tau)} \right)^2 \right\}, \quad (6.9)$$

where $\gamma \equiv 1/2 + c/\beta \approx 0.64$, and the (a priori, uncontrolled) prefactor has been chosen in such a way that the matching condition (6.3) is fulfilled exactly⁶.

The last equation suggests a remarkable simplification: Assume that k_\perp is sufficiently close to $Q_s(\tau)$ (although still above it) for $\ln(k_\perp^2/Q_s^2(\tau)) \ll \bar{\alpha}_s\tau$. Then, the second term in the exponent can be neglected compared to the first one, and eq. (6.9) reduces to

$$\lambda_\tau(k_\perp) \simeq \frac{1}{\pi} k_\perp^2 \left(\frac{Q_s^2(\tau)}{k_\perp^2} \right)^\gamma, \quad (6.10)$$

which shows *geometric scaling* : the dimensionless function $\lambda_\tau(k_\perp)/k_\perp^2$ depends upon its two variables k_\perp^2 and τ only via the combination $k_\perp^2/Q_s^2(\tau)$. Eq. (6.10) is a correct approximation for momenta k_\perp^2 within the following ‘‘scaling window’’ [18]:

$$Q_s^2(\tau) \ll k_\perp^2 \ll \frac{Q_s^4(\tau)}{Q_0^2}. \quad (6.11)$$

⁶This is, of course, just a matter of convenience; an approximate matching, as shown in eq. (6.3), would be enough for the present purposes.

The scaling form (6.10) is similar to the one derived in Ref. [18] for the dipole-hadron scattering amplitude, which reads (for $1/r_\perp^2$ within the scaling window (6.11)):

$$\mathcal{N}_\tau(r_\perp) \approx \kappa (r_\perp^2 Q_s^2(\tau))^\gamma \quad (6.12)$$

with the same exponent γ as in eq. (6.10). This exponent (or, rather, the difference $1 - \gamma$) is sometimes referred to as an “anomalous dimension” [14, 44, 22]. In fact, as we shall check in Sect. 7.2, the similitude between eqs. (6.10) and (6.12) is consistent with the linear relation (5.5) between these two quantities, valid for small r_\perp .

At this point, we should recall that geometric scaling has been first identified in the experimental data, as a regularity of the HERA data for γ^* -proton deep inelastic scattering [38]. More recently, this notion has found phenomenological applications also to electron-nucleus DIS [45], and to heavy ion collisions [46].

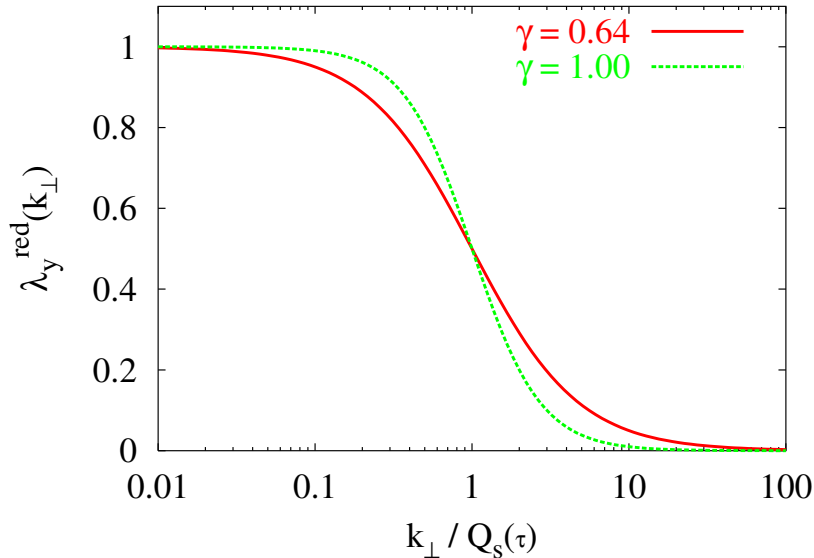


Figure 1: Momentum dependence of $\lambda_y^{\text{red}}(k_\perp) = (\pi/k_\perp^2)\bar{\lambda}_y(k_\perp)$, plotted as a function of $k_\perp/Q_s(\tau)$ for two values of γ . Solid (red) line: $\gamma = 0.64$, and dashed (green) line $\gamma = 1$.

The previous considerations show that the following scaling Ansatz for the interpolating kernel (6.2) should be a good approximation for all momenta $k_\perp \lesssim Q_s^2(\tau)/\Lambda_{QCD}$:

$$\bar{\lambda}_y(k_\perp) = \theta(\tau - y) \frac{k_\perp^2}{\pi} \frac{\left(\frac{Q_s^2(y)}{k_\perp^2}\right)^\gamma}{1 + \left(\frac{Q_s^2(y)}{k_\perp^2}\right)^\gamma}. \quad (6.13)$$

We have reintroduced here the θ -function to emphasize that the charge-charge correlator vanishes for space-time rapidities $y > \tau$. The quality of this interpolation will be tested in the next section, where we shall use eq. (6.13) to compute the dipole-hadron scattering

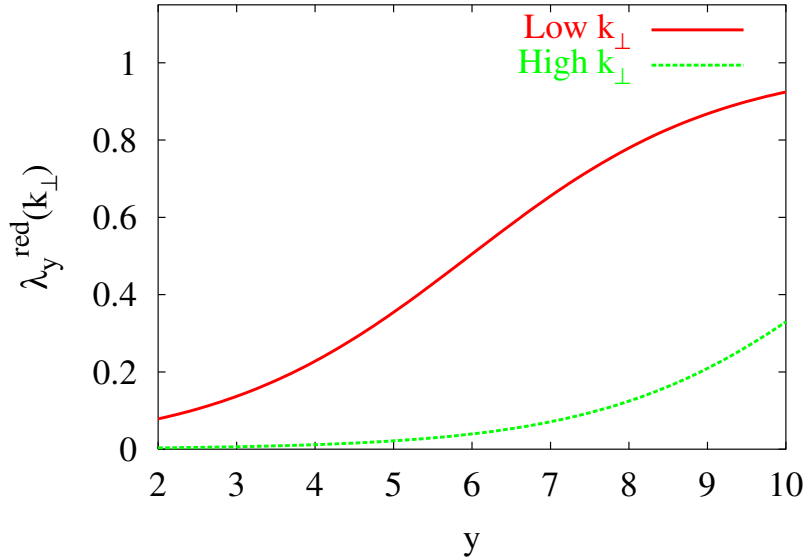


Figure 2: Longitudinal structure of $\lambda_y^{\text{red}}(k_\perp) = (\pi/k_\perp^2)\bar{\lambda}_y(k_\perp)$. This is plotted as a function of y for two transverse momenta: $k_\perp^{\text{high}} = 3Q_s^2(\tau)$ (green line, dashed), and $k_\perp^{\text{low}} = 0.02Q_s^2(\tau)$ (red line, solid). We have used $\gamma = 0.64$, $c = 4.84$, $\bar{\alpha}_s = 0.2$, and $\tau = 10$. The corresponding separation rapidities are $\tau_s(k_\perp^{\text{high}}) \simeq 11$ and $\tau_s(k_\perp^{\text{low}}) \simeq 5$.

amplitude and the unintegrated gluon distribution, and then we shall compare the results to known general properties.

In such applications, it will be convenient to treat the “anomalous dimension” γ , and also the exponent c in eq. (6.7) for the saturation scale, as free parameters. For instance, eq. (6.13) with $\gamma = 1$ provides a simple generalization of the MV model (in the sense that the transverse correlations die out at high k_\perp), but which includes the correct infrared behaviour due to saturation (thus avoiding the infrared problem of the original MV model), and also some of the quantum evolution, via the rapidity dependence of the saturation scale.

Moreover, eq. (6.13) with $\gamma = 1$ can be used as a rough approximation for the general kernel (6.2) in the DLA regime⁷ at very high transverse momenta $k_\perp \gg Q_s^2(\tau)/\Lambda_{QCD}$. Indeed, in that regime, the solution to the BFKL equation can be replaced by its DLA approximation, which has only a weak dependence upon k_\perp . This suggests that, in applications to the phenomenology, one can always use the simplified kernel (6.13), but let the anomalous dimension γ be weakly dependent upon k_\perp , in such a way that $\gamma \approx \gamma_{\text{BFKL}} \simeq 0.64$ within the scaling window (6.11), and $\gamma \approx 1$ for much larger momenta. More generally, one can imagine extracting both γ and c from fits to the experimental

⁷Note that this is the regime where the dipole–hadron scattering shows “colour transparency” [47], i.e., the corresponding scattering amplitude behaves like $\mathcal{N}_\tau(r_\perp) \sim \alpha_s r_\perp^2 xG(x, 1/r_\perp^2)/\pi R^2$, where $xG(x, Q^2)$ is the gluon distribution to be discussed in Sect. 7.1.

data. In the subsequent applications, we shall give results for both $\gamma = 1$ and $\gamma = 0.64$.

The quantity $\bar{\lambda}_y(k_\perp)$ is represented in Fig. 1 as a function of k_\perp for fixed y , and in Fig. 2 as a function of y for two values of k_\perp (one above $Q_s(\tau)$, the other one below it). For convenience, we have plotted the rescaled function $\lambda_y^{\text{red}}(k_\perp) \equiv (\pi/k_\perp^2)\bar{\lambda}_y(k_\perp)$. Note that the y dependence of $\lambda_y(k_\perp)$ represents the longitudinal profile of the colour charge distribution in the hadron, for modes of given k_\perp . (Recall that $\lambda_y(k_\perp)$ is the average colour charge squared per unit space–time rapidity per unit transverse area, for a given k_\perp .) If $k_\perp > Q_s(\tau)$, the colour charge density increases exponentially with y all the way up to the edge of the hadron (located at $y = \tau$). If $k_\perp < Q_s(\tau)$, there is an exponential increase up to the intermediate rapidity $y = \tau_s(k_\perp)$, where the gluon modes with momentum k_\perp start to be saturated (cf. eq. (5.12)); then, for rapidities $\tau_s(k_\perp) < y < \tau$, the charge density remains nearly constant. This behaviour is manifest on Fig. 2.

To conclude this section, let us indicate how the previous results change when, instead of a fixed coupling α_s , one rather uses a coupling which is running with the saturation momentum: $\alpha_s \rightarrow \alpha_s(Q_s^2)$, with $\alpha_s(Q^2) \equiv b_0/\ln(Q^2/\Lambda_{\text{QCD}}^2)$. As shown in Refs. [18, 19], the only change refers to the functional form of $Q_s^2(\tau)$, which now becomes $Q_s^2(\tau) = \Lambda_{\text{QCD}}^2 e^{\sqrt{2b_0c(\tau+\tau_0)}}$, where c is the same number as in eq. (6.7), and τ_0 is a constant. All the other results related to scaling — the value of the anomalous dimension γ and the momentum range (6.11) in which the scaling holds — remain unchanged, except for the expression of the saturation scale which enters these results. In the applications to be considered in the next section, we shall restrict ourselves to the case of a fixed coupling.

7 Some applications

In this section, we shall consider a few applications of the Gaussian effective theory with kernel (6.13). First, we shall discuss the unintegrated gluon distribution, for which we shall derive a simple analytic formula which interpolates between saturation at low momenta and BFKL evolution at high momenta, and which can be easily used in further applications. In this context, we shall briefly recall how saturation arises in the effective theory for the CGC [10], and emphasize the difference in this respect between the classical MV model [3, 4] and the full theory including quantum evolution [8]. Then, we shall use eq. (3.19) to compute the dipole–hadron scattering amplitude and study its various limits. The resulting expression has the right scaling behaviour at short distances, and the correct approach towards “blackness” at large distances, and can be easily implemented in phenomenological studies of deep inelastic scattering.

7.1 The unintegrated gluon distribution

From eqs. (6.13) and (6.7), it is easy to derive the following approximation for the quantity $\mu_\tau(k_\perp)$ which characterizes the distribution of the two-dimensional colour charge density

$\rho^a(x_\perp) \equiv \int dy \rho_y^a(x_\perp)$ (cf. eqs. (3.5)–(3.7)) :

$$\bar{\mu}_\tau(k_\perp) = \int_{-\infty}^{\tau} dy \bar{\lambda}_y(k_\perp) = \frac{k_\perp^2}{\pi\gamma c\bar{\alpha}_s} \ln \left(1 + \left(\frac{Q_s^2(\tau)}{k_\perp^2} \right)^\gamma \right). \quad (7.1)$$

This quantity is interesting for, at least, two reasons:

First, it determines the probability distribution for the colour charge density in the transverse plane (i.e., the three-dimensional distribution integrated over y) :

$$Z_\tau[\rho^a(x_\perp)] = \mathcal{N}_\tau \exp \left\{ -\frac{1}{2} \int_{x_\perp, y_\perp} \frac{\rho^a(x_\perp)\rho^a(y_\perp)}{\bar{\mu}_\tau(x_\perp, y_\perp)} \right\}. \quad (7.2)$$

This is the relevant weight function for applications which do not consider explicitly the longitudinal structure of the colour source (like the numerical simulations in Refs. [32]).

Second, eq. (7.1) provides a good approximation for the unintegrated gluon distribution in a wide range of transverse momenta. More precisely, $\bar{\mu}_\tau(k_\perp)/k_\perp^2$ coincides with the gluon distribution computed in the CGC effective theory at both high and low momenta compared to $Q_s(\tau)$, and it provides a smooth interpolation between these regimes.

To show this, we start with the definition of the gluon distribution as the Fock-space gluon density in an appropriate gauge. Consider the canonical quantization of the Yang–Mills field theory in the light cone gauge $A_a^+ = 0$ [48]. The gluon distribution $xG(x, Q^2)$ (= the number of gluons of transverse size $\Delta x_\perp \sim 1/Q$ per unit rapidity) is then obtained as [11, 10] (with $k^+ = xP^+$, $\tau = \ln(1/x)$) :

$$xG(x, Q^2) = \int d^2k_\perp \Theta(Q^2 - k_\perp^2) k^+ \frac{d^3N}{dk^+ d^2k_\perp}. \quad (7.3)$$

The quantity d^3N/d^3k , which in eq. (7.3) plays the role of the unintegrated gluon distribution, is the Fock space gluon density, which is defined in terms of the gluon creation and annihilation operators in the standard way. This can be related to the following 2–point function of the LC–gauge “electric field” F_a^{+i} :

$$\frac{d^3N}{d\tau d^2k_\perp} = \frac{1}{4\pi^3} \langle F_a^{+i}(x^+, k^+, k_\perp) F_a^{+i}(x^+, -k^+, -k_\perp) \rangle_\tau, \quad (7.4)$$

which is in turn recognized as the LC–gauge expression of a gauge–invariant correlator, which in other gauges would involve also Wilson lines in the longitudinal direction [7, 10].

In fact, in the effective theory for the CGC, one exploits this gauge freedom to rewrite the correlation function in eq. (7.4) in terms of the gauge fields in the *covariant* gauge, for which we know the weight function. Namely, we use eq. (2.5) to write:

$$\langle F_a^{+i}(\vec{x}) F_a^{+i}(\vec{y}) \rangle_\tau = \langle (U_{ab}^\dagger \partial^i \alpha^b)_{\vec{x}} (U_{ac}^\dagger \partial^i \alpha^c)_{\vec{y}} \rangle_\tau \quad (7.5)$$

with $\vec{x} = (x^-, x_\perp)$, and $U^\dagger(\vec{x})$ and $\alpha_a(\vec{x})$ given by eqs. (2.6) and (2.7), respectively. The Wilson lines in the r.h.s. of eq. (7.5) encode all the non-linearities coming from the classical field equations (2.1).

Within the Gaussian effective theory with weight function (3.1), this correlation function can be explicitly computed, with the following result [8, 10] :

$$\frac{1}{\pi R^2} \frac{d^3 N}{d\tau d^2 k_\perp} = \frac{N_c^2 - 1}{4\pi^3} \int_{-\infty}^{\tau} dy \int d^2 r_\perp e^{ik_\perp \cdot r_\perp} S_y(r_\perp) (-\nabla_\perp^2 \gamma_y(r_\perp)), \quad (7.6)$$

where $\gamma_y(r_\perp)$ is the 2-point function of the field α , eq. (3.15), and $S_y(r_\perp)$ is the 2-point function of the Wilson lines in the adjoint representation, i.e., eq. (3.19) with $C_R = N_c$.

To simplify notations, it is useful to define:

$$\varphi_\tau(k_\perp) \equiv \frac{4\pi^3}{N_c^2 - 1} \frac{1}{\pi R^2} \frac{d^3 N}{d\tau d^2 k_\perp}, \quad (7.7)$$

a quantity that we shall refer to as the “unintegrated gluon distribution” in what follows. Up to the factor $4\pi^3$, this is the number of gluons of each colour per unit rapidity per unit of transverse phase-space.

Clearly, even with the interpolation (6.13) for the kernel of the Gaussian, which implies

$$\bar{\gamma}_y(k_\perp) = \frac{1}{\pi k_\perp^2} \frac{\left(\frac{Q_s^2(y)}{k_\perp^2}\right)^\gamma}{1 + \left(\frac{Q_s^2(y)}{k_\perp^2}\right)^\gamma}, \quad (7.8)$$

(cf. eq. (3.18)) it is still not easy to perform the remaining integrations in eq. (7.6) analytically. But simpler formulae can be obtained in the limiting regimes where k_\perp is either well above, or well below, the saturation scale.

Consider the high- k_\perp regime first. Then, the integral in eq. (7.6) is dominated by small $r_\perp \ll 1/Q_s(\tau)$, so that $S_y(r_\perp) \approx 1$, and the r.h.s. of eq. (7.6) reduces to

$$\int_{-\infty}^{\tau} dy \int d^2 r_\perp e^{ik_\perp \cdot r_\perp} (-\nabla_\perp^2 \gamma_y(r_\perp)) = \int_{-\infty}^{\tau} dy k_\perp^2 \gamma_y(k_\perp) = \frac{\mu_\tau(k_\perp)}{k_\perp^2}, \quad (7.9)$$

where we have also used eqs. (3.18) and (3.7). This gives:

$$\varphi_\tau(k_\perp) \simeq \frac{\mu_\tau(k_\perp)}{k_\perp^2} \quad \text{for} \quad k_\perp \gg Q_s(\tau), \quad (7.10)$$

with $\mu_\tau(k_\perp)$ obtained as the solution to the BFKL equation (5.4). Eq. (7.10) is the standard BFKL approximation for the unintegrated gluon distribution.

The low- k_\perp case is more subtle, and we shall construct our argument in several steps:

(I) We shall see eventually that, when $k_\perp \ll Q_s(\tau)$, the dominant contribution to eq. (7.6) comes from space-time rapidities in the range $\tau_s(k_\perp) < y < \tau$, with $\tau_s(k_\perp)$ defined in eq. (5.12). In order to check this, we first evaluate the contribution of the lower rapidities, $y < \tau_s(k_\perp)$. In this range, $Q_s(y) \ll k_\perp$, and the exponential factor $e^{ik_\perp \cdot r_\perp}$

selects distances $r_\perp \lesssim 1/k_\perp \ll 1/Q_s(y)$, for which $S_y(r_\perp) \simeq 1$ to a very good accuracy. Thus, this low- y contribution is proportional to (cf. eq. (7.9))

$$\int_{-\infty}^{\tau_s(k_\perp)} dy \int d^2 r_\perp e^{ik_\perp \cdot r_\perp} (-\nabla_\perp^2 \gamma_y(r_\perp)) = \frac{\mu_\tau(k_\perp)}{k_\perp^2} \Big|_{\tau=\tau_s(k_\perp)} \sim \frac{1}{\bar{\alpha}_s}, \quad (7.11)$$

where the last estimate comes from using eq. (7.1). The contribution (7.11) is a priori large, since of order $1/\alpha_s$, but nevertheless subdominant, as we shall see.

(II) We now consider the remaining contribution, namely:

$$\int_{\tau_s(k_\perp)}^\tau dy \int d^2 r_\perp e^{ik_\perp \cdot r_\perp} S_y(r_\perp) (-\nabla_\perp^2 \gamma_y(r_\perp)), \quad (7.12)$$

where, for a typical y , $k_\perp \ll Q_s(y) \ll Q_s(\tau)$. Since $e^{ik_\perp \cdot r_\perp}$ selects relatively large distances $r_\perp \gtrsim 1/Q_s(y)$, we must consider the behaviour of the integrand for such distances. In momentum space, we have (cf. eqs. (3.18) and (5.11), or directly from eq. (7.8)) :

$$k_\perp^2 \gamma_y(k_\perp) \simeq 1/\pi, \quad \text{for} \quad k_\perp \ll Q_s(y), \quad (7.13)$$

showing that, in coordinate space, $-\nabla_\perp^2 \gamma_y(r_\perp) = \pi \delta^{(2)}(r_\perp)$. Since eq. (7.13) is just a low-momentum approximation, this simply means that the function $-\nabla_\perp^2 \gamma_y(r_\perp)$ is localized at small distances $r_\perp \lesssim 1/Q_s(y)$, with integrated weight

$$\int d^2 r_\perp (-\nabla_\perp^2 \gamma_y(r_\perp)) = 1/\pi. \quad (7.14)$$

Thus, in reality, the integration in eq. (7.12) is restricted to values $r_\perp \lesssim 1/Q_s(y)$, where we cannot compute the integrand accurately (since our approximations break down around Q_s), but where $S_y(r_\perp) \approx \delta < 1$ is essentially a number of order one. That is, we shall approximate:

$$\int_{\tau_s(k_\perp)}^\tau dy \int d^2 r_\perp e^{ik_\perp \cdot r_\perp} S_y(r_\perp) (-\nabla_\perp^2 \gamma_y(r_\perp)) \approx \frac{\delta}{\pi} \int_{\tau_s(k_\perp)}^\tau dy = \frac{\delta}{\pi} (\tau - \tau_s(k_\perp)), \quad (7.15)$$

where the number $\delta < 1$ cannot be computed in the present approximations. Since, moreover (cf. eqs. (6.7) and (5.12)):

$$\tau - \tau_s(k_\perp) = \frac{1}{c\bar{\alpha}_s} \ln \frac{Q_s^2(\tau)}{k_\perp^2}, \quad (7.16)$$

where, by assumption, $\ln(Q_s^2(\tau)/k_\perp^2) \gg 1$, it is clear that the contribution (7.15) is larger than that in eq. (7.11), and thus is the dominant contribution, as anticipated.

To conclude, at low momenta $k_\perp \ll Q_s(\tau)$, we have found:

$$\varphi_\tau(k_\perp) \simeq \delta \frac{1}{\pi c\bar{\alpha}_s} \ln \frac{Q_s^2(\tau)}{k_\perp^2}, \quad \text{for} \quad k_\perp \ll Q_s(\tau), \quad (7.17)$$

which, up to the factor δ , is the same as $\mu_\tau(k_\perp)/k_\perp^2$, with $\mu_\tau(k_\perp)$ given by its low-momentum approximation (5.13).

Eq. (7.17) exhibits *gluon saturation*. To see this, compare eqs. (7.10) and (7.17): At high momenta, $\varphi_\tau(k_\perp)$ shows an exponential increase with τ (according to the BFKL equation), and also a rapid increase with decreasing k_\perp (as a power of $1/k_\perp$), which, if extrapolated at low momenta, would generate infrared problems. But for k_\perp below $Q_s(\tau)$, $\varphi_\tau(k_\perp)$ is rather described by eq. (7.17), which shows only a *linear* increase with τ , that is, logarithmic with $1/x$ — this is *small- x saturation* —, and also a logarithmic increase with $1/k_\perp$ — this is *k_\perp -saturation*. The fact that both types of saturation occur simultaneously is consistent with the notion of “geometric scaling”: At saturation, there is only one intrinsic scale in the problem, the saturation scale, so $\varphi_\tau(k_\perp)$ can be only a function of the ratio $Q_s^2(\tau)/k_\perp^2$. Thus, a logarithmic dependence upon k_\perp entails necessarily a similar behaviour in $\tau \propto \ln Q_s^2(\tau)$. As we have seen in Sect. 6, the scaling property characteristic of saturation is preserved by the BFKL evolution until relatively large values of k_\perp .

At this point, let us also emphasize a crucial difference between the saturation mechanisms in the MV model and in the full effective theory, with quantum evolution included. In the MV model, k_\perp -saturation occurs as well [3, 4], but only as a consequence of the non-linear effects in the classical field equations (2.1). That is, this classical saturation relies crucially on the presence of the Wilson lines in eq. (7.5), or of their 2-point function $S_y(r_\perp)$ in eq. (7.6).

On the other hand, these Wilson lines played almost no role in the quantum calculation leading to eq. (7.17) (they are just responsible for the overall factor δ). In this case, the saturation is rather the consequence of the long-range correlations among the colour sources, as encoded in the low- k_\perp behaviour of the function $\mu_\tau(k_\perp)$ (cf. eqs. (5.13) and (7.16)). These correlations ensure the global neutrality of the colour sources at the scale $1/Q_s(\tau)$, and this in turn implies the saturation of the radiated gluons *independently* of the non-linear effects in the classical field dynamics. The relevant non-linear effects are rather those in the quantum evolution, i.e., in the RGE (2.8), which generate the scale $Q_s(\tau)$ in the first place, as the scale for colour neutrality.

These considerations explain why there is no contradiction, in this quantum context, between having an expression for the unintegrated gluon distribution which is *linear* in $\mu_\tau(k_\perp)$ both at high momenta and at low momenta, as we have found before, and which nevertheless shows saturation. This further implies that it is enough to dispose of a good approximation for the 2-point function $\mu_\tau(k_\perp)$, namely eq. (7.1), to immediately deduce an equally good approximation for the unintegrated gluon distribution, that is,

$$\bar{\varphi}_\tau(k_\perp) \equiv \frac{\bar{\mu}_\tau(k_\perp)}{k_\perp^2} = \frac{1}{\pi\gamma c\bar{\alpha}_s} \ln \left(1 + \left(\frac{Q_s^2(\tau)}{k_\perp^2} \right)^\gamma \right). \quad (7.18)$$

At low momenta, $k_\perp \ll Q_s(\tau)$, this clearly reproduces the behaviour in eq. (7.17) (except for the factor δ , which is unknown anyway, and will be ignored in what follows). At high

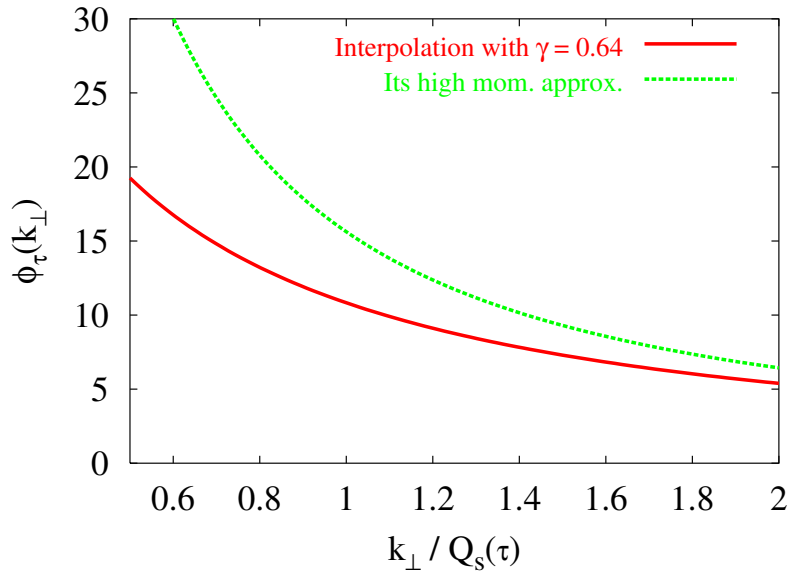


Figure 3: $\bar{\varphi}_\tau(k_\perp)$ as a function of $k_\perp/Q_s(\tau)$ in linear scale (red line, solid), compared with its high momentum approximation $(Q_s^2(\tau)/k_\perp^2)^\gamma$ (green line, dashed). We have used $\bar{\alpha}_s = 0.1$ and $\gamma = 0.64$.

momenta, $k_\perp \gg Q_s(\tau)$,

$$\bar{\varphi}_\tau(k_\perp) \simeq \frac{1}{\pi\gamma c\bar{\alpha}_s} \left(\frac{Q_s^2(\tau)}{k_\perp^2} \right)^\gamma, \quad (7.19)$$

which is the geometric scaling version of the BFKL expression in eq. (7.10), and therefore holds, strictly speaking, only within the scaling window (6.11).

According to (7.18), the saturation condition can be also formulated in terms of φ_τ : $Q_s(\tau)$ is the scale at which the unintegrated gluon distribution becomes of order $1/\bar{\alpha}_s$:

$$\varphi_\tau(k_\perp) \sim \frac{1}{\bar{\alpha}_s} \quad \text{for} \quad k_\perp \sim Q_s(\tau). \quad (7.20)$$

The k_\perp -dependence of the function (7.18) is illustrated in Figs. 3, 4 and 5, by using both linear and logarithmic scales, so that the various regimes alluded to before become manifest. In particular, in Fig. 5, we have indicated also the τ -dependence of the result, by plotting $\bar{\varphi}_\tau(k_\perp)$ as a function of k_\perp for several values of τ .

7.2 The dipole–hadron scattering amplitude

After using eq. (7.1), the S -matrix element for dipole–hadron scattering, eq. (3.19), becomes [for a gluonic dipole, i.e., with $C_R = N_c$] :

$$S_\tau(r_\perp) = \exp \left\{ -\frac{4\pi}{\gamma c} \int \frac{d^2 k_\perp}{(2\pi)^2} \frac{1 - e^{ik_\perp \cdot r_\perp}}{k_\perp^2} \ln \left[1 + \left(\frac{Q_s^2(\tau)}{k_\perp^2} \right)^\gamma \right] \right\} \equiv e^{-\Omega_\tau(r_\perp)}. \quad (7.21)$$

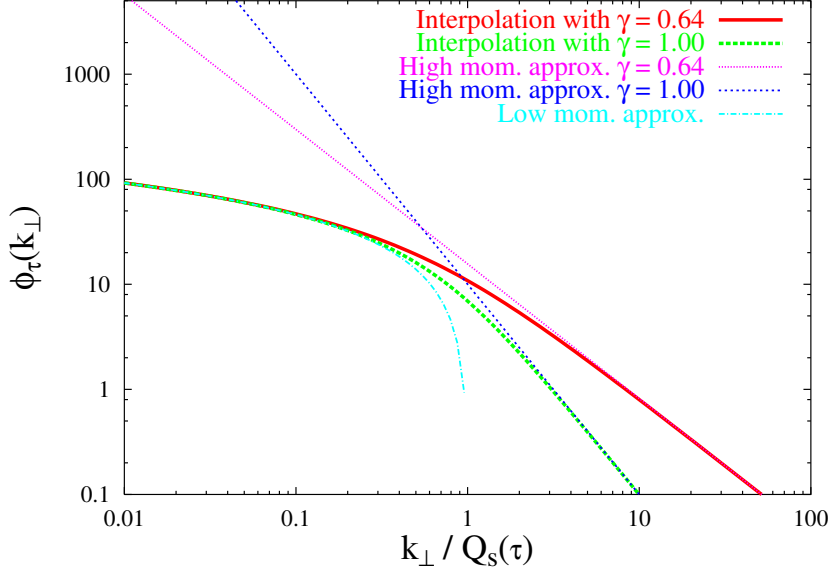


Figure 4: $\bar{\varphi}_\tau(k_\perp)$ as a function of $k_\perp/Q_s(\tau)$ in log–log scale for two values of γ : $\gamma = 0.64$ (red line, thick solid), and $\gamma = 1$ (green line, thick dashed). Comparison is made with $1/k_\perp^{2\gamma}$, $\gamma = 0.64$ (magenta line, thin dotted), $1/k_\perp^2$ (blue line, thin dashed), and $(1/\bar{\alpha}_s) \ln(Q_s^2(\tau)/k_\perp^2)$ (cyan line, thin dot–dashed).

Clearly, for any $\gamma > 0$, the integral in the exponent is both ultraviolet and infrared finite, so, by dimensional analysis, its result must be a scaling function (i.e., a function of $r_\perp Q_s(\tau)$). In what follows, we shall study the asymptotic behaviour of this function for both $r_\perp Q_s(\tau) \ll 1$ (small dipole) and $r_\perp Q_s(\tau) \gg 1$ (large dipole). This is interesting for several reasons: *i*) It allows us to identify the dominant scattering mechanisms in these limits. *ii*) It illustrates the role of saturation in providing a smoother infrared behaviour, and thus infrared finite results (this will be especially clear in the comparison with the MV model for $\gamma = 1$). *iii*) For a small dipole and $\gamma < 1$, we shall verify explicitly that the anomalous dimension γ is correctly transmitted from the kernel of the Gaussian to the scattering amplitude (cf. eq. (6.12)). *iv*) For a large dipole, we shall recognize the behaviour expected from previous studies of the BK equation [22, 11], and of the RGE (2.8) [8, 10]). Also, we shall present the results of the numerical evaluation of eq. (7.21) for two values of γ .

(I) Short-range behaviour: $r_\perp \ll 1/Q_s(\tau)$

To estimate the integral in eq. (7.21), we divide the integration range into three domains separated by the external scales $1/r_\perp$ and $Q_s(\tau)$. Thus, we need to consider the following domains: (I–a) $1/r_\perp \ll k_\perp$, (I–b) $Q_s(\tau) \ll k_\perp \ll 1/r_\perp$, and (I–c) $k_\perp \ll Q_s(\tau)$.

In domain (I–a), k_\perp is the largest scale in the problem, so $k_\perp \cdot r_\perp \gg 1$ and $Q_s^2(\tau)/k_\perp^2 \ll 1$. Then, one can ignore the rapidly oscillating exponential $e^{ik_\perp \cdot r_\perp}$, and also expand the

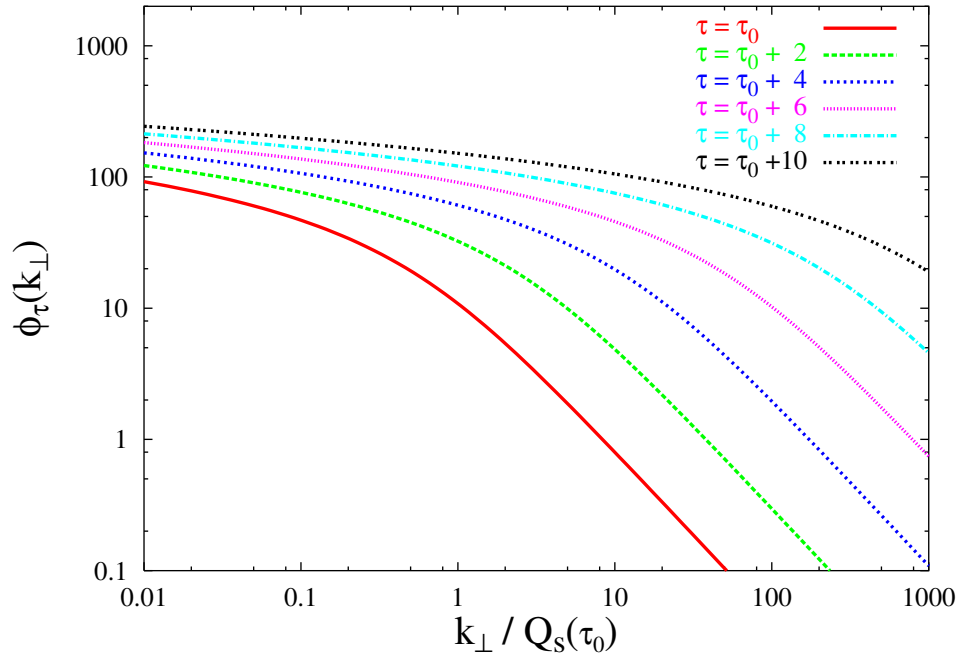


Figure 5: Energy dependence of $\bar{\varphi}_\tau(k_\perp)$ for $\gamma = 0.64$. We have plotted $\varphi_\tau(k_\perp)$ as a function of $k_\perp/Q_s(\tau_0)$ (with τ_0 some value of reference) for six values of τ . The lines, from the bottom to the top, correspond successively to $\tau = \tau_0, \tau_0 + 2, \dots, \tau_0 + 10$. The increase with τ is exponential at high momenta (giving equidistant curves in this log-log plot), but only logarithmic at low momenta.

logarithm as $\ln(1+x) \simeq x$. This gives:

$$\Omega^{(I-a)} \simeq \frac{1}{\gamma c} \int_{1/r_\perp}^{\infty} \frac{dk_\perp^2}{k_\perp^2} \left(\frac{Q_s^2(\tau)}{k_\perp^2} \right)^\gamma = \frac{1}{\gamma^2 c} (r_\perp^2 Q_s^2(\tau))^\gamma. \quad (7.22)$$

In domain (I-b), one can expand both the logarithm, as above, and the exponential, and keep only the leading term which survives after the angular integral. That is, we can replace $1 - e^{ik_\perp \cdot r_\perp} \rightarrow \frac{1}{4} r_\perp^2 k_\perp^2$, and thus obtain:

$$\Omega^{(I-b)} \simeq \frac{1}{4\gamma c} r_\perp^2 \int_{Q_s^2(\tau)}^{1/r_\perp^2} dk_\perp^2 \left(\frac{Q_s^2(\tau)}{k_\perp^2} \right)^\gamma \simeq \begin{cases} \frac{1}{4c} r_\perp^2 Q_s^2(\tau) \ln(1/r_\perp^2 Q_s^2(\tau)) & \text{for } \gamma = 1 \\ a (r_\perp^2 Q_s^2(\tau))^\gamma & \text{for } \gamma < 1 \end{cases} \quad (7.23)$$

with $a = 1/[4c\gamma(1-\gamma)]$. Note that the case $\gamma = 1$ requires a separate treatment.

Lastly, in domain (I-c), we can expand the exponential as above, and approximate $\ln(1+x) \simeq \ln x$. We obtain:

$$\Omega^{(I-c)} \simeq \frac{1}{4c} r_\perp^2 \int_0^{Q_s^2(\tau)} dk_\perp^2 \ln \left(\frac{Q_s^2(\tau)}{k_\perp^2} \right) = \frac{1}{4c} r_\perp^2 Q_s^2(\tau). \quad (7.24)$$

Putting the results altogether, it is clear that, when $\gamma = 1$, the leading contribution comes from domain (I-b), since this is enhanced by a large logarithm. This gives:

$$S_\tau(r_\perp) \Big|_{\gamma=1} \simeq \exp \left\{ -\frac{1}{4c} r_\perp^2 Q_s^2(\tau) \ln \frac{1}{r_\perp^2 Q_s^2(\tau)} \right\}, \quad (7.25)$$

which is formally similar to the MV model (compare to eq. (4.8)), with the crucial difference, however, that the scale in the logarithm is now set by the (hard) saturation momentum $Q_s(\tau)$, rather than by Λ_{QCD} . This reflects the fact that, due to colour neutrality at saturation, the quantum effective theory is free of infrared problems.

Note also that the exponent in eq. (7.25) vanishes at $r_\perp = 1/Q_s(\tau)$, which indicates that this expression is valid only at very short distances, $r_\perp \ll 1/Q_s(\tau)$, and thus cannot be used to study the approach towards saturation. For this latter purpose, a more refined calculation is necessary, and for $\gamma = 1$, this can be even performed analytically. We shall return to this calculation towards the end of the section.

When $\gamma < 1$, on the other hand, it is clear from eqs. (7.22) and (7.23) that domains (I-a) and (I-b) contribute on the same footing, and give together the leading behaviour. This shows that the integral in eq. (7.21) is now dominated by momenta $k_\perp \sim 1/r_\perp$, as expected for the BFKL dynamics. We thus deduce that, for $r_\perp \ll 1/Q_s(\tau)$ (but within the scaling window (6.11)), the scattering amplitude has the right scaling form:

$$\mathcal{N}_\tau(r_\perp) \approx \Omega_\tau(r_\perp) \Big|_{\gamma < 1} \simeq \kappa (r_\perp^2 Q_s^2(\tau))^\gamma \quad (7.26)$$

(with κ some unknown number) in agreement with eq. (6.12).

Note that k_\perp is the momentum transferred between the incoming dipole, of transverse size r_\perp , and the colour sources that it scatters off in the hadronic target. Thus, the

previous discussion shows that a small dipole ($r_\perp \ll 1/Q_s(\tau)$) undergoes mostly *hard* scattering ($k_\perp \gg Q_s(\tau)$), that is, it interacts predominantly with the colour sources in its vicinity in the impact parameter space. This agrees with the conclusions in Ref. [9].

(II) Long distance behaviour: $r_\perp \gg 1/Q_s(\tau)$

The three domains that we have to consider now are: (II-a) $k_\perp \gg Q_s(\tau)$, (II-b) $Q_s(\tau) \gg k_\perp \gg 1/r_\perp$, and (II-c) $1/r_\perp \gg k_\perp$. Their respective contributions are easily estimated, with the following results:

$$\Omega^{(\text{II-a})} \simeq \frac{1}{\gamma c} \int_{Q_s^2(\tau)}^{\infty} \frac{dk_\perp^2}{k_\perp^2} \left(\frac{Q_s^2(\tau)}{k_\perp^2} \right)^\gamma = \frac{1}{\gamma^2 c}, \quad (7.27)$$

$$\Omega^{(\text{II-b})} \simeq \frac{1}{c} \int_{1/r_\perp^2}^{Q_s^2(\tau)} \frac{dk_\perp^2}{k_\perp^2} \ln \left(\frac{Q_s^2(\tau)}{k_\perp^2} \right) = \frac{1}{2c} \left(\ln r_\perp^2 Q_s^2(\tau) \right)^2, \quad (7.28)$$

$$\Omega^{(\text{II-c})} \simeq \frac{1}{4c} r_\perp^2 \int_0^{1/r_\perp^2} dk_\perp^2 \ln \left(\frac{Q_s^2(\tau)}{k_\perp^2} \right) \simeq \frac{1}{4c} \ln r_\perp^2 Q_s^2(\tau). \quad (7.29)$$

Clearly, to leading-log accuracy, the dominant contribution comes from domain (II-b), and gives:

$$S_\tau(r_\perp) \propto \exp \left\{ -\frac{1}{2c} \left(\ln r_\perp^2 Q_s^2(\tau) \right)^2 \right\}, \quad (7.30)$$

in agreement with the results in Refs. [22, 8, 10, 11]. In this case, the dipole scattering is dominated by relatively long-range interactions ($k_\perp \ll Q_s(\tau)$, with $k_\perp \gg 1/r_\perp$ though), that is, by the interactions with the saturated gluons.

Eq. (7.30) describes the approach of the S -matrix element towards the “black disk” limit $S_\tau(r_\perp) = 0$ in the regime where the dipole is already very large. Thus, when this functional form starts to apply, $S_\tau(r_\perp)$ is already significantly smaller than one (i.e., the proportionality coefficient in eq. (7.30) should be rather small).

Let us finally return to the case $\gamma = 1$, and show that, in this case, the behaviour of $S_\tau(r_\perp)$ around the saturation scale can be studied analytically. To this aim, it is preferable to return to the expression of $S_\tau(r_\perp)$ in eq. (3.19) [with $\bar{\lambda}_y(k_\perp)$ as given by eq. (6.13)], and perform first the momentum integration there, for fixed y . This generates a modified Bessel function (see the Appendix for more details), which is then expanded in an infinite series, and the result is integrated over y term by term. The final result reads:

$$\Omega_\tau(r_\perp) \Big|_{\gamma=1} = \frac{4}{c} \sum_{n=1}^{\infty} \frac{(Q_s^2(\tau)r^2)^n}{(n!)^2 4^n 2n} \left\{ \left(\frac{1}{2n} + \psi(n+1) + \ln 2 \right) - \frac{1}{2} \ln(Q_s^2(\tau)r^2) \right\}. \quad (7.31)$$

By using this exact series expansion, one can study the approach towards saturation from shorter distances. Namely, for $r_\perp \ll 1/Q_s(\tau)$, the dominant contribution comes from the $n = 1$ term in eq. (7.31), which yields

$$S_\tau^{\text{short}}(r_\perp) \Big|_{\gamma=1} \simeq \exp \left\{ -\frac{1}{4c} Q_s^2(\tau)r^2 \left[\ln \frac{1}{Q_s^2(\tau)r^2} + \left(1 + 2\psi(2) + 2 \ln 2 \right) \right] \right\}. \quad (7.32)$$

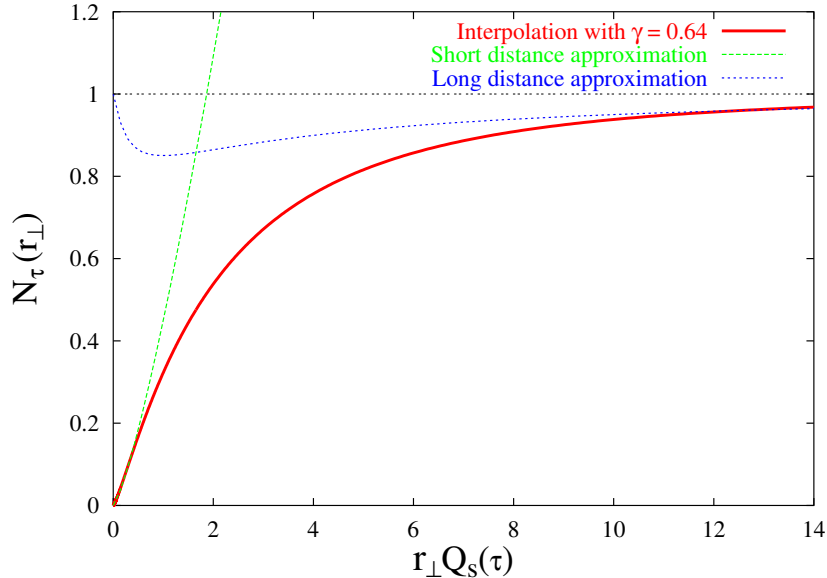


Figure 6: The scattering amplitude $1 - S_\tau(r_\perp)$ for $\gamma = 0.64$ plotted as a function of $r_\perp Q_s(\tau)$. Red solid line: numerical evaluation of eq. (7.21); green dashed line: short distance approximation, eq. (7.26); blue dotted line: long distance approximation, eq. (7.30).

As compared to the leading-log result in eq. (7.25), the expression above displays also the subleading term under the logarithm. Clearly, when r_\perp approaches $1/Q_s(\tau)$ from below, this formally “subleading” term gives the dominant behaviour.

In Figs. 6 and 7, we represent the results of the numerical evaluation of the scattering amplitude $\mathcal{N}_\tau(r_\perp) = 1 - S_\tau(r_\perp)$, eq. (7.21), for two values of the anomalous dimension: $\gamma = 0.64$ (Fig. 6) and $\gamma = 1$ (Fig. 7). In the same plots, we display, for comparison, the corresponding predictions of the various approximations derived previously in this subsection.

8 Conclusions and perspectives

In this paper, we have proposed a simple Gaussian approximation for the weight function for the effective Colour Glass description of the small- x gluons in the hadron wavefunction. The main virtue of this approximation is its simplicity. The new weight function is as simple to use in practice as that of the original McLerran–Venugopalan model, but it improves over the latter by including the correlations among the colour sources associated with quantum evolution towards small x and gluon saturation. This ensures, in particular, the removal of the infrared divergences inherent to the MV model, without invoking non-perturbative physics: Gauge-invariant observables come out infrared finite because of the colour neutrality of the saturated gluons over the (relatively short) scale $1/Q_s(\tau)$. More

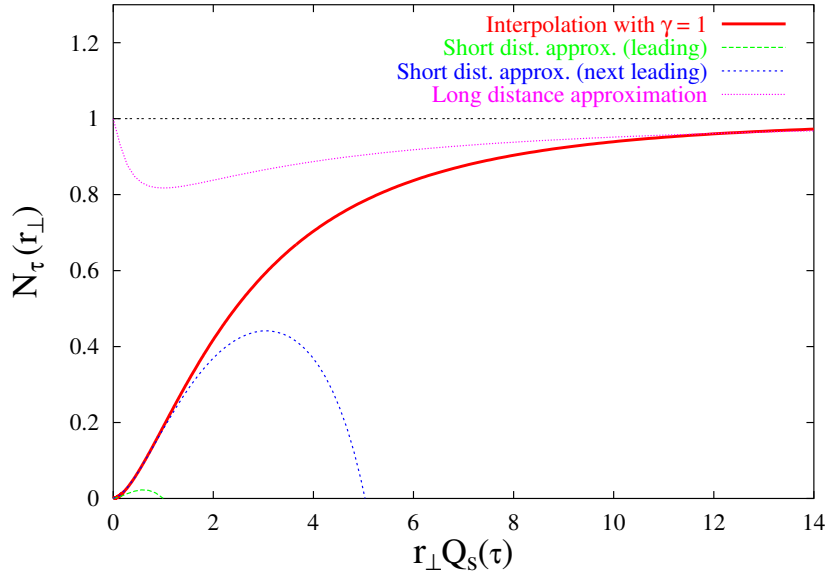


Figure 7: The scattering amplitude $1 - S_\tau(r_\perp)$ for $\gamma = 1$ plotted as a function of $r_\perp Q_s(\tau)$. Red solid line: numerical evaluation of eq. (7.21); green dashed line: leading-order short distance approximation, eq. (7.25); blue dotted line: next-to-leading-order short distance approximation, eq. (7.32); magenta dotted line: long distance approximation, eq. (7.30).

generally, this Gaussian weight function implements the BFKL dynamics (for both the gluon distribution, and the dipole-hadron scattering) at high transverse momenta, and gluon saturation at low transverse momenta, with the change between these two regimes taking place at the saturation scale, as it should.

In its simplest form, the kernel of the Gaussian is a scaling function, eq. (6.13), which is strictly valid up to momenta $k_\perp \lesssim Q_s^2(\tau)/\Lambda_{QCD}$, and involves three dimensionless parameters: the anomalous dimension γ , the logarithmic derivative of the saturation momentum $\lambda \equiv d \ln Q_s^2(\tau)/d\tau$ (throughout this paper, we have rather denoted this quantity as $\lambda = c\bar{\alpha}_s$; see, e.g., eq. (6.7)), and the initial rapidity $\tau_0 = \ln(1/x_0)$ which appears when the saturation momentum, eq. (6.7), is rewritten as $Q_s^2(x) = Q_0^2 e^{\lambda(\tau-\tau_0)} \equiv Q_0^2 (x_0/x)^\lambda$, with Q_0 some convenient scale of reference (e.g., $Q_0 = 1$ GeV). Of course, within the present approximations, the values of γ and λ are determined by the leading-order BFKL dynamics. But since we expect geometric scaling and the exponential rise of the saturation scale with τ to be more general than just LO BFKL, we can also treat these quantities as free parameters, to be fitted from the data, or taken from some more refined calculations. For instance, the fits to the electron-proton deep inelastic scattering data at HERA using the “saturation model” [39, 40] provide a value $\lambda \simeq 0.3$, which, remarkably, appears to be consistent with a recent calculation [20] of the saturation scale using the NLO BFKL dynamics [49] (with the RG-improved kernel proposed in Refs. [50]).

The Gaussian weight function that we have constructed and justified here can be

immediately used to supplant the MV model in its applications to the physics at small x .

For the problems involving only one high-density hadronic system (one large nucleus⁸, or a very energetic hadron), the calculations can be performed quasi-analytically, since the solution to the corresponding classical field equations is known in analytic form (cf. Section 2.1). This includes various studies of proton-nucleus (pA) collisions [4, 51, 52, 53], or of ultra-peripheral nucleus-nucleus (AA) collisions [54]. Also, the expression for the dipole-hadron scattering amplitude that we have obtained in this context, eq. (7.21), can be used in analyses of the DIS data at HERA, as an alternative to the more phenomenological parametrizations proposed in Refs. [39, 40]. It would be interesting, in this respect, to compare eq. (7.21) with the numerical solution of the BK equation [22, 23, 24, 25], or with the results of the lattice simulations of the full RGE [55] (the latter should be soon available [56]). We expect our analytic formula (7.21) to be numerically close to such more complete calculations, while being much simpler to use in practice, and allowing for the freedom to choose (or fit) the values of the parameters γ and λ (in the numerical calculations alluded to above, these parameters are rather fixed to their respective BFKL values, by the dynamics of the relevant equations).

For applications of the CGC effective theory to heavy ion collisions, the classical field equations can be numerically solved on a lattice, as in Refs. [32], and their results averaged over the colour charge distributions in the incoming nuclei, with the Gaussian weight function. As compared to the MV model, the use of the new Gaussian in such applications would eliminate the sensitivity to the poorly known non-perturbative physics. Still within the context of AA collisions, we note that the simple analytic form we have derived for the unintegrated gluon distribution, eq. (7.18), can be directly implemented in analytic calculations of the multiparticle production, like those in Refs. [46, 57].

Acknowledgments

We would like to thank Miklos Gyulassy for having triggered this work with his incentive remarks, and Al Mueller for illuminating discussions on the implications of color neutrality for the calculation of the gluon distribution function. We are grateful to François Gelis for helping us with the numerical calculations, and for a very careful reading of the manuscript, with many useful remarks.

This manuscript has been authorized under Contracts No. DE-AC02-8-CH10886 and No. DE-AC02-76CH0300 with the US Department of Energy.

⁸For applications involving large nuclei, one needs also to compute, or parametrize, the A -dependence of the saturation scale. One expects a power-law increase, $Q_s^2(\tau, A) \propto A^\delta$, with $\delta \simeq 1/3$ (see, e.g., [45, 46]).

A Appendix

In this Appendix, we derive the analytic expression (7.31) for the exponent of the S -matrix element, which refers to eq. (7.21) with $\gamma = 1$. We first perform the momentum integration in eq. (3.19), where $\lambda_y(k_\perp)$ is now replaced by its interpolation in eq. (6.13) (with $\gamma = 1$). It is useful to decompose this latter as follows:

$$\frac{1}{k_\perp^4} \bar{\lambda}_y(k_\perp) \Big|_{\gamma=1} = \frac{1}{\pi} \left[\frac{1}{k_\perp^2} - \frac{1}{k_\perp^2 + Q_s^2(y)} \right]. \quad (\text{A.1})$$

When this function is inserted in the integrand of eq. (3.19), its product with $1 - e^{ik_\perp \cdot r_\perp}$ is naturally decomposed into four terms. Since the overall integral is finite, we are allowed to evaluate these four terms separately, provided we use the same regularization scheme. All these terms are represented by a simple integral (after angular integration, $r = |r_\perp|$):

$$\int_0^\infty dk J_0(kr) \frac{k}{k^2 + P^2} = K_0(Pr), \quad (\text{A.2})$$

where $K_0(z)$ is the modified Bessel function (with $\psi(z) = d \ln \Gamma(z)/dz$)

$$K_0(z) = -\ln z + (\ln 2 - \gamma) + \sum_{n=1}^{\infty} \frac{1}{(n!)^2} \left(\frac{z}{2}\right)^{2n} \left(\psi(n+1) - \ln \frac{z}{2}\right). \quad (\text{A.3})$$

For example, the term $\int (d^2 k_\perp/k_\perp^2)$, which has both ultraviolet and infrared divergences, can be regularized as $\int 2\pi k dk J_0(k/\Lambda)/(k^2 + \mu^2)$, with Λ and μ being the UV and IR cutoffs, respectively, and thus brought into the form of eq. (A.2). When adding the contributions of the four terms, all divergences cancel out, as they should, and, in the limit $\Lambda \rightarrow \infty$ and $\mu \rightarrow 0$, we are left with the following result:

$$\Omega_\tau(r_\perp) \Big|_{\gamma=1} = 2\bar{\alpha}_s \int_{-\infty}^{\tau} dy \left\{ \ln(Q_s(y)r) - (\ln 2 - \gamma) + K_0(Q_s(y)r) \right\}. \quad (\text{A.4})$$

The integral over the rapidity y can be now performed, by using the energy dependence of $Q_s(y)$ given in eq. (6.7) :

$$\begin{aligned} \Omega_\tau(r_\perp) \Big|_{\gamma=1} &= \frac{4}{c} \int_0^{Q_s(\tau)r} \frac{d\zeta}{\zeta} \left\{ \ln \zeta - (\ln 2 - \gamma) + K_0(\zeta) \right\} \quad [\zeta = Q_s(y)r] \\ &= \frac{4}{c} \int_0^{Q_s(\tau)r} d\zeta \sum_{n=1}^{\infty} \frac{1}{(n!)^2} \frac{1}{\zeta} \left(\frac{\zeta}{2}\right)^{2n} \left\{ \psi(n+1) - \ln \frac{\zeta}{2} \right\}. \end{aligned} \quad (\text{A.5})$$

In the last line, we have used eq. (A.3). By integrating this series term by term, one obtains the final result in eq. (7.31).

References

- [1] L. McLerran and R. Venugopalan, *Phys. Rev.* **D49** (1994) 2233; *ibid.* **49** (1994) 3352; *ibid.* **50** (1994) 2225.
- [2] Yu.V. Kovchegov, *Phys. Rev.* **D54** (1996), 5463; *Phys. Rev.* **D55** (1997), 5445.
- [3] J. Jalilian-Marian, A. Kovner, L. McLerran, H. Weigert, *Phys. Rev.* **D55** (1997) 5414.
- [4] Yu.V. Kovchegov and A.H. Mueller, *Nucl. Phys.* **B529** (1998), 451.
- [5] C. S. Lam and G. Mahlon, *Phys. Rev.* **D62** (2000) 114023; *ibid.* **D64** (2001) 016004.
- [6] J. Jalilian-Marian, A. Kovner, A. Leonidov and H. Weigert, *Nucl. Phys.* **B504** (1997) 415; *Phys. Rev.* **D59** (1999) 014014.
- [7] E. Iancu, A. Leonidov and L. McLerran, *Nucl. Phys.* **A692** (2001), 583; *Phys. Lett.* **B510** (2001) 133; E. Ferreiro, E. Iancu, A. Leonidov and L. McLerran, *Nucl. Phys.* **A703** (2002) 489.
- [8] E. Iancu and L. McLerran, *Phys. Lett.* **B510** (2001) 145.
- [9] E. Ferreiro, E. Iancu, K. Itakura, and L. McLerran, *Nucl. Phys.* **A710** (2002) 373.
- [10] E. Iancu, A. Leonidov and L. McLerran, *The Colour Glass Condensate: An Introduction*, hep-ph/0202270. Published in *QCD Perspectives on Hot and Dense Matter*, pp. 73–146, NATO Science Series, Kluwer, 2002.
E. Iancu, hep-ph/0210236, invited talk at Quark Matter 2002 (QM 2002), Nantes, France, 18–24 July 2002.
- [11] A. H. Mueller, *Small-x Physics, High Parton Densities and Parton Saturation in QCD*, hep-ph/9911289. Published in *Lisbon 1999, QCD: Perturbative or nonperturbative ?*, pp. 180–209;
Parton Saturation—An Overview, hep-ph/0111244. Published in *QCD Perspectives on Hot and Dense Matter*, pp. 45–72, NATO Science Series, Kluwer, 2002.
- [12] J.-P. Blaizot, E. Iancu, and H. Weigert, hep-ph/0206279, to appear in *Nucl.Phys.* **A**.
- [13] L.N. Lipatov, *Sov. J. Nucl. Phys.* **23** (1976) 338; E.A. Kuraev, L.N. Lipatov and V.S. Fadin, *Zh. Eksp. Teor. Fiz* **72**, 3 (1977) (*Sov. Phys. JETP* **45** (1977) 199); Ya.Ya. Balitsky and L.N. Lipatov, *Sov. J. Nucl. Phys.* **28** (1978) 822.
- [14] L.V. Gribov, E.M. Levin, and M.G. Ryskin, *Phys. Rept.* **100** (1983) 1.
- [15] A.H. Mueller and J. Qiu, *Nucl. Phys.* **B268** (1986) 427.
- [16] J.-P. Blaizot and A. H. Mueller, *Nucl. Phys.* **B289** (1987) 847.

- [17] A. H. Mueller, *Nucl. Phys.* **B558** (1999) 285.
- [18] E. Iancu, K. Itakura, and L. McLerran, *Nucl. Phys.* **A708** (2002) 327.
- [19] A. H. Mueller and D.N. Triantafyllopoulos, *Nucl. Phys.* **B640** (2002) 331.
- [20] D.N. Triantafyllopoulos, *The Energy Dependence of the Saturation Momentum from RG Improved BFKL Evolution*, hep-ph/0209121.
- [21] Yu. V. Kovchegov, *Phys. Rev.* **D60** (1999), 034008; *ibid.* **D61** (2000) 074018.
- [22] E. Levin and K. Tuchin, *Nucl. Phys.* **B573** (2000) 833; *Nucl. Phys.* **A691** (2001) 779; *Nucl. Phys.* **A693** (2001) 787.
- [23] N. Armesto and M. Braun, *Eur. Phys. J.* **C20** (2001) 517; *ibid.* **C22** (2001) 351.
- [24] K. Golec-Biernat, L. Motyka, and A.M. Staśto, *Phys. Rev.* **D65** (2002) 074037.
- [25] E. Levin and M. Lublinsky, *Phys. Lett.* **B521** (2001) 233; *Eur. Phys. J.* **C22** (2002) 647; M. Lublinsky, *Eur. Phys. J.* **C21** (2001) 513.
- [26] I. Balitsky, *Nucl. Phys.* **B463** (1996) 99; *High-energy QCD and Wilson lines*, hep-ph/0101042.
- [27] A. H. Mueller, *Nucl. Phys.* **B335** (1990) 115.
- [28] A. H. Mueller, *Nucl. Phys.* **B415** (1994) 373; *ibid.* **B437** (1995) 107.
- [29] M. Braun, *Eur. Phys. J.* **C16** (2000) 337.
- [30] H. Weigert, *Nucl. Phys.* **A703** (2002) 823.
- [31] A. H. Mueller, *Phys. Lett.* **B523** (2001) 243.
- [32] A. Krasnitz, R. Venugopalan, *Phys. Rev. Lett.* **84** (2000) 4309; *ibid.* **86** (2001) 1717; A. Krasnitz, Y. Nara, and R. Venugopalan, *ibid.* **87** (2001) 192302; hep-ph/0209269.
- [33] A. H. Mueller, *Nucl. Phys.* **B643** (2002) 501.
- [34] E.M. Levin and M.G. Ryskin, *Phys. Rept.* **189** (1990) 267.
- [35] A. Kovner and U.A. Wiedemann, *Phys. Rev.* **D66** (2002) 034031.
- [36] M. Froissart, *Phys. Rev.* **123** (1961) 1053.
- [37] M. Kozlov and E. Levin, *QCD Saturation and $\gamma^* - \gamma^*$ Scattering*, hep-ph/0211348.
- [38] A.M. Staśto, K. Golec-Biernat, and J. Kwieciński, *Phys. Rev. Lett.* **86** (2001) 596.

- [39] K. Golec-Biernat, M. Wüsthoff, *Phys. Rev.* **D59** (1999) 014017; **D60** (1999) 114023.
- [40] J. Bartels, K. Golec-Biernat, and H. Kowalski, *Phys. Rev.* **D66** (2002) 014001.
- [41] N.N. Nikolaev and B.G. Zakharov, *Z. Phys.* **C49** (1991) 607, *ibid.* **C53** (1992) 331.
- [42] W. Buchmuller, M.F. McDermott and A. Hebecker, *Nucl. Phys.* **B487** (1997) 283, Erratum-*ibid.* **B500** (1997) 621; W. Buchmuller, T. Gehrmann, and A. Hebecker *Nucl. Phys.* **B537** (1999) 477.
- [43] V.N. Gribov and L.N. Lipatov, *Sov. Journ. Nucl. Phys.* **15** (1972), 438; G. Altarelli and G. Parisi, *Nucl. Phys.* **B126** (1977), 298; Yu. L. Dokshitzer, *Sov. Phys. JETP* **46** (1977), 641.
- [44] J. Bartels and E. Levin, *Nucl. Phys.* **B387** (1992) 617.
- [45] A. Freund, K. Rummukainen, H. Weigert, and A. Schaefer, *Geometric scaling in inclusive e A reactions and nonlinear perturbative QCD*, hep-ph/0210139.
- [46] D. E. Kharzeev, E. Levin, and L. McLerran, hep-ph/0210332.
- [47] B. Blättel, G. Baym, L.L. Frankfurt, and M. Strikman, *Phys. Rev. Lett.* **70** (1993) 896.
- [48] J.B. Kogut and D.E. Soper, *Phys. Rev.* **D1** (1970) 2901.
- [49] V.S. Fadin and L.N. Lipatov, *Phys. Lett.* **B429** (1998) 127; G. Camici and M. Ciafaloni, *Phys. Lett.* **B430** (1998) 349.
- [50] G.P. Salam, *JHEP* **9807** (1998) 19; M. Ciafaloni, D. Colferai, *Phys. Lett.* **B452** (1999) 372; M. Ciafaloni, D. Colferai, and G.P. Salam, *Phys. Rev.* **D60** (1999) 114036.
- [51] A. Dumitru and L. McLerran, *Nucl. Phys.* **A700** (2002) 492.
- [52] A. Dumitru and J. Jalilian-Marian, *Phys. Rev. Lett.* **89** (2002) 022301.
- [53] F. Gelis and J. Jalilian-Marian, *Phys. Rev.* **D66** (2002) 014021; *ibid.* 094014.
- [54] F. Gelis and A. Peshier, *Nucl. Phys.* **A697** (2002) 879; *ibid.* **A707** (2002) 175.
- [55] K. Rummukainen and H. Weigert, in preparation.
- [56] H. Weigert, private communication.
- [57] D. Kharzeev and M. Nardi, *Phys. Lett.* **B507** (2001) 121; D. E. Kharzeev and E. Levin, *Phys. Lett.* **B523** (2001) 79.